



Human Cytomegalovirus Uses a Host Stress Response To Balance the Elongation of Saturated/Monounsaturated and Polyunsaturated Very-Long-Chain Fatty Acids

Yuecheng Xi,^a Lena Lindenmayer,^b Ian Kline,^a  Jens von Einem,^b  John G. Purdy^{a,c,d}

^aDepartment of Immunobiology, University of Arizona, Tucson, Arizona, USA

^bInstitute of Virology, Ulm University Medical Center, Ulm, Germany

^cBIO5 Institute, University of Arizona, Tucson, Arizona, USA

^dCancer Biology Interdisciplinary Program, University of Arizona, Tucson, Arizona, USA

ABSTRACT Stress and virus infection regulate lipid metabolism. Human cytomegalovirus (HCMV) infection induces fatty acid (FA) elongation and increases the abundance of lipids with very-long-chain FA (VLCFA) tails. While reprogramming of metabolism can be stress related, the role of stress in HCMV reprogramming of lipid metabolism is poorly understood. In this study, we engineered cells to knock out protein kinase R (PKR)-like endoplasmic reticulum kinase (PERK) in the ER stress pathway and measured lipid changes using lipidomics to determine if PERK is needed for lipid changes associated with HCMV infection. In HCMV-infected cells, PERK promotes increases in the levels of phospholipids with saturated FA (SFA) and monounsaturated FA (MUFA) VLCFA tails. Further, PERK enhances FA elongase 7 (ELOVL7) protein levels, which elongates SFA and MUFA VLCFAs. Additionally, we found that increases in the elongation of polyunsaturated fatty acids (PUFAs) associated with HCMV infection were independent of PERK and that lipids with PUFA tails accumulated in HCMV-infected PERK knockout cells. Additionally, the protein levels of ELOVL5, which elongates PUFAs, are increased by HCMV infection through a PERK-independent mechanism. These observations show that PERK differentially regulates ELOVL7 and ELOVL5, creating a balance between the synthesis of lipids with SFA/MUFA tails and PUFA tails. Additionally, we found that PERK was necessary for virus replication and the infectivity of released viral progeny. Overall, our findings indicate that PERK—and, more broadly, ER stress—may be necessary for the membrane biogenesis needed to generate infectious HCMV virions.

IMPORTANCE HCMV is a common herpesvirus that establishes lifelong persistent infections. While infection is asymptomatic in most people, HCMV causes life-threatening illnesses in immunocompromised people, including transplant recipients and cancer patients. Additionally, HCMV infection is a leading cause of congenital disabilities. HCMV replication relies on lipid synthesis. Here, we demonstrated that the ER stress mediator PERK controls FA elongation and the cellular abundance of several types of lipids following HCMV infection. Specifically, PERK promotes FA elongase 7 synthesis and phospholipids with saturated/monounsaturated very-long-chain FA tails. Overall, our study shows that PERK is an essential host factor that supports HCMV replication and promotes lipidome changes caused by HCMV infection.

KEYWORDS ER stress, PERK, fatty acid elongases, herpesviruses, human cytomegalovirus, lipidomics, lipids, very-long-chain fatty acids

Regulation of metabolism in response to acute and chronic external or internal stressors allows cells to adapt to stressful situations, including viral infections (1–6). Human cytomegalovirus (HCMV) reprograms metabolism, in part by inducing stress

Citation Xi Y, Lindenmayer L, Kline I, von Einem J, Purdy JG. 2021. Human cytomegalovirus uses a host stress response to balance the elongation of saturated/monounsaturated and polyunsaturated very-long-chain fatty acids. *mBio* 12:e00167-21. <https://doi.org/10.1128/mBio.00167-21>.

Editor Thomas Shenk, Princeton University

Copyright © 2021 Xi et al. This is an open-access article distributed under the terms of the [Creative Commons Attribution 4.0 International license](https://creativecommons.org/licenses/by/4.0/).

Address correspondence to John G. Purdy, jgpurdy@arizona.edu.

Received 20 January 2021

Accepted 27 March 2021

Published 4 May 2021

responses, to create a metabolic state that supports virus replication (7, 8). The endoplasmic reticulum (ER) has roles in both lipid metabolism and stress. The integrated stress response, lipid synthesis, and protein translation and folding take place in the ER. Disruption of ER homeostasis triggers a stress response that can include activating protein kinase R (PKR)-like ER kinase (PERK; also known as eukaryotic translation initiation factor 2 α kinase 3 [EIF2AK3]). PERK reduces ER stress related to the accumulation of misfolded proteins by inactivating EIF2 α through phosphorylation to decrease translation. PERK has an emerging role in lipid metabolism as well. PERK-mediated lipogenesis supports the proper development of lipid-generating tissues, such as adipocytes and mammary glands (9). In the context of viral infection, PERK is needed for HCMV-induced lipid synthesis (7, 10). However, the effects of PERK on specific classes or types of lipids in HCMV-infected cells remain unknown.

HCMV infection induces several lipogenic enzymes, including those involved in fatty acid (FA) synthesis and elongation (8, 10–14), which are required for HCMV replication (10, 12–14). FAs have several functions as free fatty acids or as hydrophobic tails in lipids, including establishing and maintaining membrane integrity. The function of FAs depends on their length and the number and placement of double bonds in the hydrocarbon chain. HCMV infection promotes the synthesis of lipids with very-long-chain fatty acid (VLCFA) tails containing 24 or more carbons with no double bonds (i.e., saturated fatty acids [SFAs]) or one double bond (i.e., monounsaturated fatty acids [MUFAs]) (13, 14). In HCMV-infected cells, SFAs are made by fatty acid elongase 7 (ELOVL7) (13). Humans encode seven ELOVLs that elongate FAs based on the chain length and double bond content (15–19). The expression of ELOVLs is regulated by sterol regulatory-element binding proteins (SREBPs), liver X receptor α (LXR α), and peroxisome proliferation-activated receptor α (PPAR α) (20). However, little is known concerning mechanisms involved in the differential expression of ELOVLs (i.e., how a cell may regulate ELOVL7 differently than ELOVL5).

We recently demonstrated that HCMV UL37x1 protein (pUL37x1; also known as viral mitochondria-localized inhibitor of apoptosis [vMIA]) helps to support HCMV enhancement of SFA elongation and synthesis of phospholipids (PLs) with VLCFA (PL-VLCFA) tails (8). Additionally, pUL37x1 helps to increase PERK protein levels following infection (8). In this study, we investigated the role of PERK in the biogenesis of different lipid classes in response to HCMV infection. We engineered PERK knockout (KO) cells using CRISPR/Cas9 and performed several lipidomic analyses to define lipids regulated by PERK following HCMV infection. We expanded on our previous PL lipidomic work by including the analysis of diglycerides (DGs) and triglycerides (TGs). HCMV infection increases the relative levels of most DGs and TGs with SFA/MUFA VLCFA tails. We found that PERK affects the levels of PLs, DGs, and TGs, specifically in the double bond content of their tails. Our findings reveal that PERK balances the ratio of lipids with SFA/MUFA VLCFA tails and lipids with polyunsaturated fatty acid (PUFA) tails. Moreover, we show that in HCMV-infected cells, PERK differentially regulates ELOVLs involved in SFA/MUFA and PUFA elongation. Our study provides a new perspective on how HCMV remodels the host lipidome and how cellular stress regulates FA elongation and balances SFAs/MUFAs and PUFAs.

RESULTS

HCMV infection promotes PERK to support virus replication. HCMV infection with the lab-adapted AD169 strain increases PERK protein levels in primary human fibroblasts under the fully confluent, serum-free conditions used in our metabolism studies (8, 13). We examined whether infection with the low-passage-number, more clinically relevant TB40/E strain would also enhance PERK protein levels under the same cell culture conditions. PERK protein levels in uninfected and TB40/E-infected cells were measured following infection at a multiplicity of infection (MOI) of 1 infectious unit (IU) per cell. PERK protein levels increased as early as 4 h postinfection (hpi) and remained elevated through 96 hpi, with the highest levels observed at 24 to 72 hpi (Fig. 1A and B). Next, we

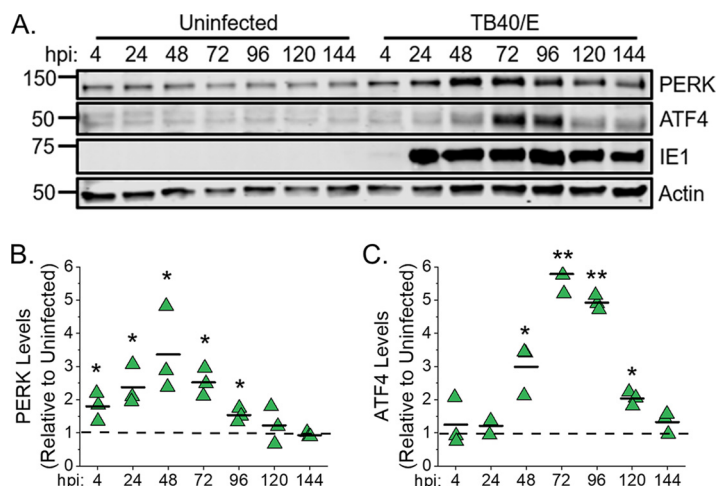


FIG 1 HCMV infection upregulates PERK and ATF4 protein levels. (A) Western blot analysis of PERK and ATF4 protein levels in uninfected and HCMV TB40/E-infected fibroblast cells at a multiplicity of infection (MOI) of 1 infectious unit per cell. Numbers at the left are molecular masses (in kilodaltons). (B, C) Quantification of PERK and ATF4 protein levels following normalization to the actin level. The value for PERK or ATF4 at each time point is shown relative to the level in uninfected cells at the same time point. A dashed line represents the level in uninfected cells, and each data point from three independent experiments is shown with the mean represented as a bar. *, $P < 0.05$; **, $P < 0.01$; paired-sample *t* test. $n = 3$.

examined whether PERK is activated in HCMV-infected cells by measuring ATF4 protein levels, a transcription factor that is increased by PERK activity. ATF4 levels were enhanced in HCMV-infected cells relative to its levels in uninfected cells at 48 to 120 hpi (Fig. 1A and C). ATF4 protein was highest at 72 hpi, with a 5.5-fold-higher level in HCMV-infected cells than in uninfected cells. Our findings that HCMV infection enhances PERK protein levels and activity is consistent with those of others who reached the same conclusion using other HCMV strains or cell types (5, 7, 8, 21, 22).

To investigate possible functions of PERK in HCMV-infected cells, we generated PERK knockout (PERK-KO) clones using CRISPR/Cas9 and two independent guide RNAs (gRNAs) (see Fig. S1A to C in the supplemental material). Each PERK-KO clone was generated by single-cell cloning using human foreskin fibroblast (HFF) cells exogenously expressing human telomerase. CRISPR/Cas9 gene editing was identified using indel sequencing. Clone 1 (PERK-KO-c1) has a 300-bp deletion in exon 1 that removed the start codon for PERK translation (Fig. S1A and B). Clone 2 (PERK-KO-c2) contains a 4-bp deletion after the PERK translation start site that introduces a frameshift, leading to a premature stop codon. The loss of PERK protein was confirmed using Western blotting (Fig. S1C). We generated CRISPR/Cas9-expressing control cells that contain a nontargeting (NT) gRNA sequence that lacks the ability to target any human or HCMV gene. The NT cells were single-cell cloned in parallel with the PERK-KO cells. Individual NT clones were pooled to limit off-target effects from CRISPR/Cas9 cloning.

The loss of PERK in the KO cells was further confirmed in HCMV-infected cells using Western blotting. TB40/E-infected PERK-KO cells failed to express PERK (Fig. 2A). Next, we evaluated PERK activity in the KO cells by measuring the levels of ATF4 in TB40/E-infected cells. At 72 and 96 hpi, the levels of ATF4 protein were lower in HCMV-infected PERK-KO cells than in infected NT cells (Fig. 2A and B). The decrease in ATF4 protein levels confirms the loss of PERK activity in the KO cells.

The KO cells were used to determine whether PERK is required for HCMV replication by infecting PERK-KO and NT cells with TB40/E at an MOI of 1. Since TB40/E infectious virus is both cell associated and extracellularly released, we measured total virus production (i.e., cell-associated and released virions). At 120 and 144 hpi, infectious viral progeny was measured by determining the 50% tissue culture infectious dose (TCID₅₀).

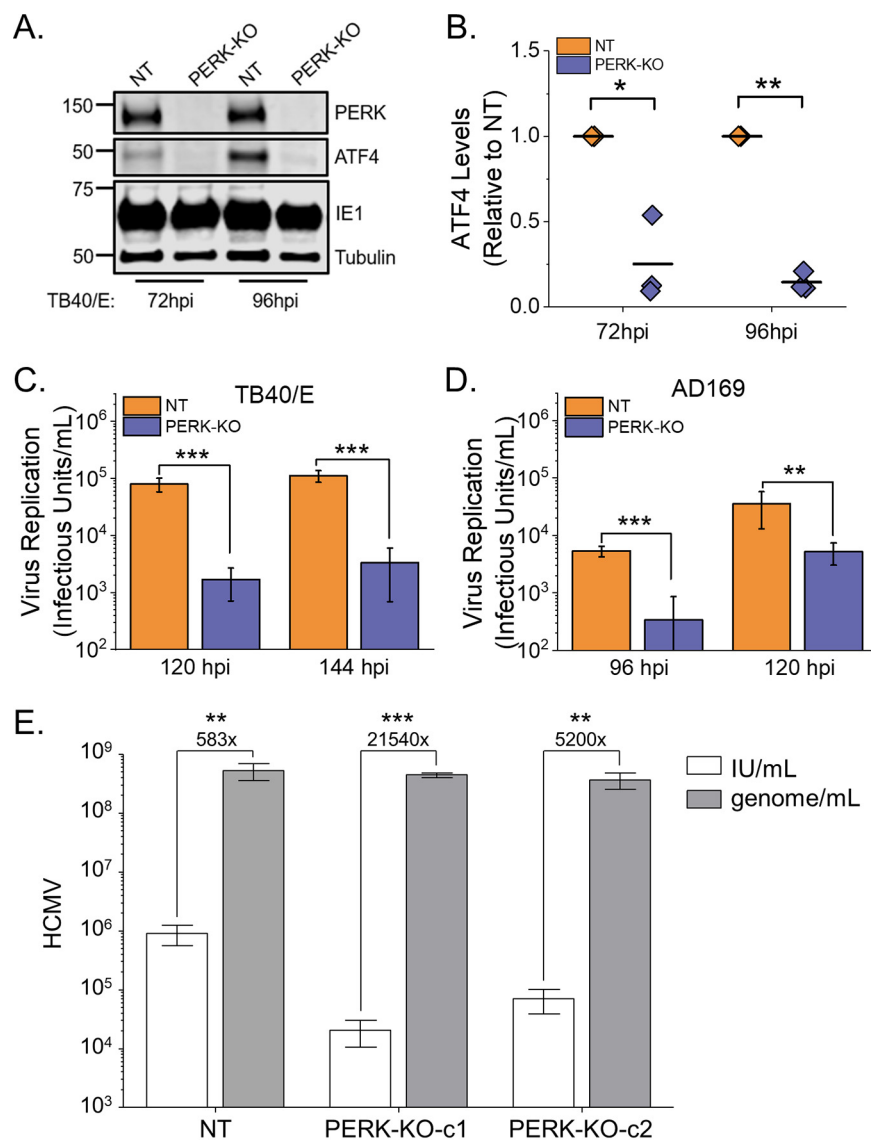


FIG 2 PERK enhances HCMV replication. (A) Western analysis of PERK and ATF4 protein levels in PERK-KO-c1 and NT cells infected at an MOI of 1. (B) Quantification of ATF4 protein levels following normalization to tubulin protein levels. The value for ATF4 is shown relative to the level in TB40/E-infected NT cells. Each data point from three independent experiments is shown, with the mean represented as a bar. (C) PERK-KO-c1 and NT cells were infected with TB40/E at an MOI of 1. The number of infectious intracellular and extracellular viruses was measured at 120 hpi and 144 hpi by determining the TCID₅₀. (D) The release of infectious virus particles was assayed by infecting PERK-KO-c1 and NT cells with AD169 at an MOI of 1. At 96 hpi and 120 hpi, infectious extracellular virus released into the growth medium was measured by determining the TCID₅₀. (E) Virus yields in cell-free supernatants were determined at 144 hpi following an infection at an MOI of 3 (white bars). In the same supernatants, the number of genome-containing particles released by cells was measured by qPCR (gray bars). The genome-to-infectious unit (IU) ratio was determined, and the values are listed above the bars. *, $P < 0.05$; **, $P < 0.01$; ***, $P < 0.001$. (B) One-sample t test. (C to E) Two-sample t test. $n = 3$.

TB40/E virus progeny production was >10 -fold lower in PERK-KO cells than in NT control cells (Fig. 2C). We further defined the impact of PERK on HCMV infection by measuring virus cell-to-cell spread using a focus expansion assay. In this assay, cells were infected with 100 infectious HCMV virions, and at 24 hpi, the cells were overlaid with methylcellulose to limit virus spread from released particles. At 9 days postinfection (dpi), HCMV-infected cells were visualized using immunofluorescence microscopy after staining them for immediate-early protein 1 (IE1), and the number of infected cells per

plaque was determined. NT control cells had a mean of 38 HCMV-infected cells per plaque (Fig. S1D). In contrast, HCMV formed smaller foci, with a mean of 21 infected cells per plaque in PERK-KO cells.

Next, we addressed the possibility that PERK may support the release of infectious progeny. We first addressed this possibility using the AD169 strain since AD169 virions are more efficiently released by infected fibroblasts than TB40/E virions. We used the TCID₅₀ to measure the amount of infectious virus released at 96 and 120 hpi by infecting NT and PERK-KO cells at an MOI of 1. PERK-KO-c1 cells released infectious AD169 virus progeny at a level 10-fold lower than that in NT cells (Fig. 2D). The release of AD169 progeny was also lower in PERK-KO-c2 cells than in NT cells (Fig. S1E). We further confirmed these findings using cells infected at an MOI of 3 with TB40/E to increase the amount of released virus. At 144 hpi, PERK-KO cells infected at an MOI of 3 released >10-fold-fewer infectious virus particles than NT cells did (Fig. 2E, white bars), consistent with our findings using AD169.

Our observations suggest that PERK-KO cells release fewer infectious virus particles or that the released virus particles are less infectious than the virus particles made by NT cells. First, we examined the possibility that PERK supports HCMV release by measuring the total number of genome-containing viral particles released into the growth medium. At 144 hpi, the supernatant from PERK-KO and NT cells was collected, and the number of genomes present was determined by quantitative PCR (qPCR). The number of genome-containing virus particles released by PERK-KO cells was similar to that in NT cells (Fig. 2E, gray bars). This finding indicates that PERK is not required for the production and release of virus particles. Next, we determined whether the virus particles released by PERK-KO cells are less infectious than those released by NT cells to assess whether PERK affects HCMV infectivity. Therefore, we calculated the ratio of genome-containing particles to infectious units (i.e., genome-to-IU ratio). The genome-to-IU ratio was around 580 in the control cells (Fig. 2E). In the PERK-KO cells, the genome-to-IU ratio was between 5,200 and 21,540. A higher ratio represents reduced particle infectivity. Since the genome-to-IU ratio was 8- to 36-fold greater in the PERK-KO cells than in the control cells, our findings indicate that PERK-KO cells release virus particles with reduced infectivity.

We conclude that PERK is necessary for efficient HCMV replication and the infectivity of released viral progeny. Moreover, our observations using CRISPR/Cas9-engineered PERK-KO cells are consistent with those of short-hairpin RNA (shRNA) PERK knockdown cells (7), providing support that our observed phenotypes are due to the loss of PERK activity and not due to our genetic engineering approach.

HCMV infection elevates the levels of DGs and TGs. ER stress induced by viral and noninfectious diseases regulates lipid metabolism through PERK activity (7, 9, 23, 24). Prior to determining the role of PERK in the lipid metabolism of HCMV-infected cells, we further defined the effects of infection on lipids. HCMV infection promotes lipid synthesis and increases the intracellular concentration of several lipid classes (7, 8, 10, 13, 25, 26). We have previously shown that HCMV increases the concentration of phospholipids, particularly those with phospholipid VLCFA (PL-VLCFA) tails (8). However, the levels of diglycerides (DGs) and triglycerides (TGs), including those with VLCFA tails, have been studied less. DG lipids are comprised of two FA tails attached to a glycerol lipid backbone. DGs are intermediates in the synthesis of both phospholipids and TG lipids. TGs have three FA tails attached to a glycerol backbone, allowing these molecules to store FAs that can be used when needed. We identified and quantitatively measured the relative levels of DGs and TGs in HCMV-infected and uninfected cells using liquid chromatography–high-resolution tandem mass spectrometry (LC-MS/MS). Since DGs and TGs are neutral lipids, sodiated and ammoniated adducts formed during electrospray ionization were used to identify and quantitate their levels. First, the levels of DGs and TGs were visualized in HCMV-infected cells relative to those in uninfected cells using a plot where each adduct form is represented by a dot (Fig. 3). In these dot plots, the DG or TG levels in infected cells are on the y axis, and the levels

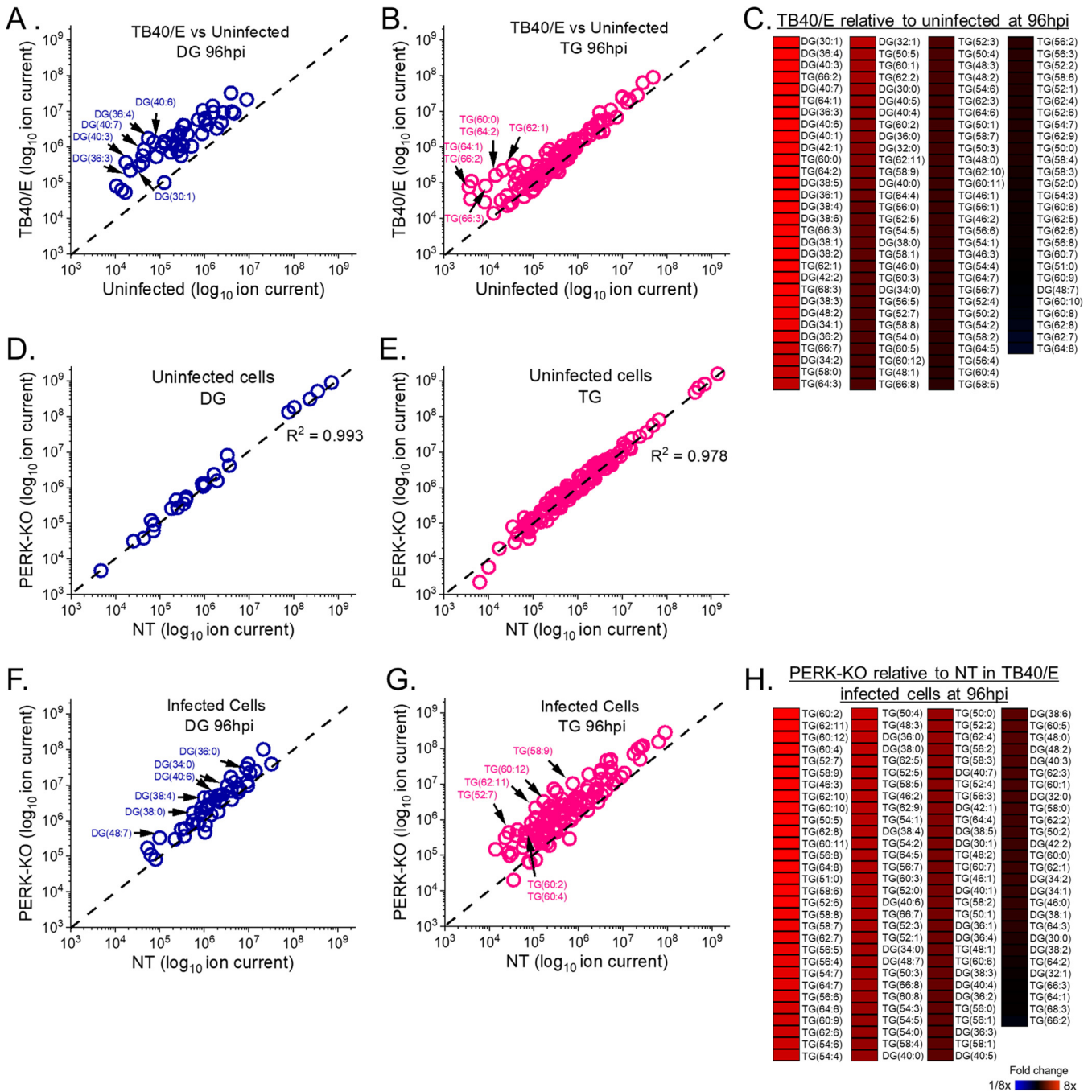


FIG 3 HCMV infection elevates diglycerides (DGs) and triglycerides (TGs), which are further increased by the loss of PERK. (A) Relative levels of DGs in TB40/E-infected cells and uninfected cells at 96 hpi. Sodiated and ammoniated adducts of DGs were measured by liquid chromatography high-resolution tandem mass spectrometry (LC-MS/MS) using electrospray ionization (ESI) following normalization by cell number. Each dot in the plot represents the level of an adduct form of a DG lipid in TB40/E-infected cells relative to its level in uninfected cells. The dashed line represents a relative level of 1 (i.e., the level in infected cells is equal to the level in uninfected cells). (B) Relative levels of TGs in TB40/E-infected cells and uninfected cells at 96 hpi. TG data were analyzed and visualized using the same methods described for panel A. (C) Changes in the relative levels of DGs and TGs in cells were quantified by averaging the relative levels of the sodiated and ammoniated adducts if both were measured. The averaged relative fold changes were log transformed and are visualized as a heatmap. (D, E) Relative levels of DGs and TGs in uninfected PERK-KO and NT cells. (F to H) Relative levels of DGs and TGs in TB40/E-infected PERK-KO and NT cells at 96 hpi. DGs and TGs were analyzed and visualized as described for panels A to C. All cells were infected at MOI of 3. $n = 3$.

in uninfected cells are on the x axis. If the level of a DG or TG is the same in HCMV-infected and uninfected cells, then its dot will fall along the dashed linear line shown in each dot plot. At 96 hpi, most DGs are above the line, demonstrating that their levels are greater in TB40/E-infected cells than in uninfected cells (Fig. 3A). Since all DGs,

except for one, were elevated in HCMV-infected cells at 96 hpi, we examined earlier time points to determine when DG levels are altered by infection. At 48 hpi, approximately 35% of DGs were more abundant in infected cells than in uninfected cells (Fig. S2A). At 72 hpi, approximately 75% of DGs were more abundant (≥ 2 -fold) in HCMV-infected cells than in uninfected cells (Fig. S2D). Next, we examined whether AD169 infection alters the levels of DGs. At 72 hpi, the level of most DGs was greater in AD169-infected cells than in uninfected cells (Fig. S2G), similar to what occurs with TB40/E-infected cells at 72 and 96 hpi. In summary, HCMV infection increases the cellular levels of DGs by 48 hpi, and their levels continue to rise through 96 hpi.

Since DGs form an intermediate step in the synthesis of TGs, the increased levels of DGs following HCMV infection may suggest that the levels of TGs may be altered by infection. At 96 hpi, $\sim 20\%$ of TGs were more abundant (≥ 2 -fold) in TB40/E-infected cells than in uninfected cells (Fig. 3B). At 48 and 72 hpi, the levels of 14 to 20% of TGs were elevated in HCMV-infected cells relative to levels in uninfected cells, respectively (Fig. S2B and E). Most of the TGs whose levels were increased by HCMV [e.g., TG(62:1), TG(62:2), and TG(64:2)] were elevated at all time points examined, indicating that they are increased by 48 hpi and remained elevated during virus replication. Several of the same TGs were more abundant in AD169-infected cells than in uninfected cells at 72 hpi (Fig. S2H).

The dot plots visualize multiple adduct forms of DGs and TGs. To provide a more quantitative analysis when both the sodiated and ammoniated adduct forms were observed by LC-MS/MS, we averaged the relative fold changes of their levels in infected and uninfected cells. The averaged relative fold changes were visualized using heatmaps. As the dot plots predicted, most DGs and TGs were > 2 -fold higher in TB40/E-infected cells than in uninfected cells at 96 hpi (Fig. 3C). More specifically, the abundances of all DGs, except DG(48:7), and of $\sim 20\%$ of TGs were ≥ 2 -fold higher in TB40/E-infected cells than in uninfected cells at 96 hpi. Similarly, DGs and TGs tended to be elevated in TB40/E-infected cells at 48 and 72 hpi and in AD169-infected cells (Fig. S2C, F, and I).

PERK KO increases the levels of several DGs and TGs in HCMV-infected cells. We examined whether PERK is required for the changes in DG and TG levels associated with HCMV infection by comparing the relative abundances of DGs and TGs in PERK-KO cells to those in NT cells. First, we determined whether the loss of PERK affects DG and TG levels in uninfected cells under our experimental conditions, where cells were at full confluence and in serum-free growth medium. There was minimal difference in the levels of DGs and TGs between uninfected PERK-KO and NT cells (Fig. 3D and E). Next, we examined whether the loss of PERK affects DG and TG levels in HCMV-infected cells. We infected PERK-KO and NT control cells with TB40/E at an MOI of 3. Again, we visualized the data using dot plots. In this case, the level of a DG or TG in infected PERK-KO cells is on the y axis, and its level in infected NT cells is on the x axis. At 96 hpi, many dots representing DGs are above the dashed line, indicating that several DGs were more abundant in HCMV-infected PERK-KO cells than in infected NT cells (Fig. 3F). However, several dots fall along or near the dashed line, indicating that the loss of PERK did not raise the relative level of all DGs above the abundance observed in HCMV-infected cells. Like the DGs, the relative abundances of several but not all TGs were higher in HCMV-infected PERK-KO cells than in infected NT cells at 96 hpi (Fig. 3G). Overall, the abundances of approximately 65% of DGs and 80% of TGs were ≥ 2 -fold higher in HCMV-infected PERK-KO cells than in infected NT cells (Fig. 3H). Likewise, most DGs and TGs were elevated in TB40/E-infected PERK-KO cells at 48 and 72 hpi (Fig. S3A to F). These findings indicate that levels of some DGs and TGs increased by HCMV infection (Fig. 3A and B) are further enhanced in infected PERK-KO cells (Fig. 3F and G). Next, we determined whether PERK is required for changes in DG and TG levels following infection with AD169. In contrast to TB40/E infection, the levels of several DGs in AD169-infected PERK-KO cells were lower than in infected NT cells

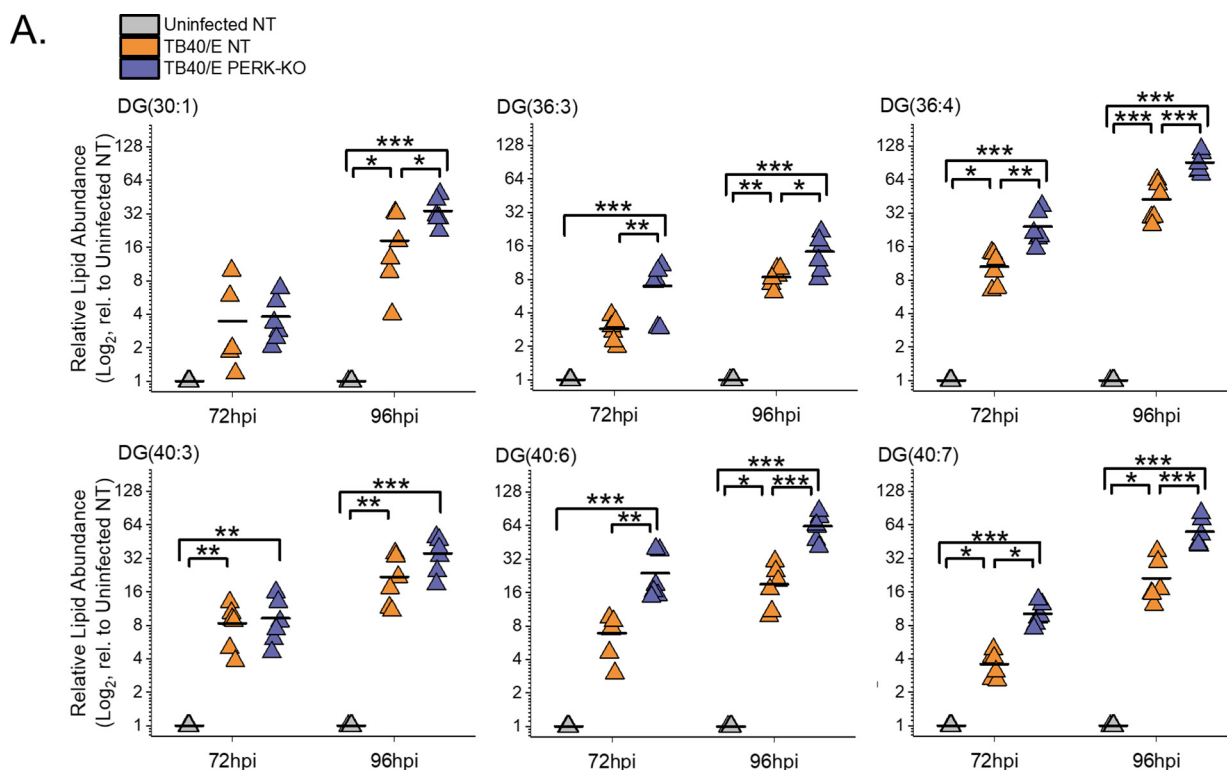
(Fig. S3G). However, AD169-infected PERK-KO cells had higher levels of TGs than infected NT cells did, similar to the findings for TB40/E-infected cells (Fig. S3H and I).

Overall, the results show that HCMV infection increases the abundances of DGs and TGs. The loss of PERK further promotes an increase in some lipids in TB40/E-infected cells. The observations presented in Fig. 3 and Fig. S2 and S3 further suggest that the level of DGs may be HCMV strain dependent, depending on the presence of PERK.

HCMV infection elevates the levels of DGs with PUFA tails. Our findings related to DGs described above show that HCMV infection increases the relative abundances of most DG lipids. We sought to understand better whether the DGs altered the most by HCMV infection were of a specific type. To address this, we examined the top six DGs whose levels were altered the greatest by TB40/E infection using the quantitative measurements visualized in our heatmaps. We further examined the top six DGs increased by infection, as shown in the heatmap in Fig. 3C. At 96 hpi, the relative abundances of these six DGs were 10- to 40-fold greater in TB40/E-infected cells than in uninfected cells (Fig. 4A). Most of these DGs contained polyunsaturated fatty acid (PUFA) tails, which have two or more double bonds (Fig. 4B). The PUFA tails had 3 to 6 double bonds and ranged in length from 20 to 22 carbons. While the relative abundances of these six DGs were greater in HCMV-infected cells than in uninfected cells at 96 hpi, only half were increased at 72 hpi, suggesting that the DG levels in HCMV-infected cells are dynamic during HCMV replication. In contrast to TB40/E infection, the DGs increased the most by AD169 infection contained saturated fatty acid (SFA) tails, i.e., those with no double bonds, or monounsaturated fatty acid (MUFA) tails, i.e., those with one double bond (Fig. S2G). However, it is noteworthy that in the AD169 experiments, fewer DGs with PUFA tails were measured than in the TB40/E experiments. These findings suggest that some DGs may be regulated in a strain-specific manner. Nonetheless, we conclude that at late time points in virus replication, TB40/E infection increases the levels of most DGs, and those with PUFA tails are elevated the greatest.

Loss of PERK elevates the levels of DGs regardless of their tail composition. Since HCMV-infected cells have elevated levels of DGs with PUFA tails, we sought to determine whether PERK influences the levels of DGs with PUFA tails during infection. Examination of the six DGs increased the most by HCMV infection (from Fig. 3C) revealed that their levels were further elevated in TB40/E-infected PERK-KO cells relative to levels in infected NT cells and uninfected cells (Fig. 4A). Most of these DGs were more abundant in PERK-KO cells than in infected NT control cells and uninfected cells at 72 and 96 hpi (Fig. 4A). As described above, most of these DGs have PUFA tails, suggesting that the loss of PERK leads to an accumulation of lipids with PUFA tails in HCMV-infected cells (Fig. 4B). Next, we determined whether the loss of PERK would elevate other types of DGs, such as those with SFA or MUFA tails. We examined this possibility by identifying the tail compositions of the six DGs that were increased the most by the loss of PERK in HCMV-infected cells at 96 hpi (these are the top DGs shown in the heatmap in Fig. 3H). At 96 hpi, the relative abundances of these six DGs were 2- to 6-fold greater in infected PERK-KO cells than in infected NT cells and 2.5- to 60-fold more abundant than in uninfected cells (Fig. 5A). Half of these DGs have PUFA tails, and the other half have SFA tails (Fig. 5B). Together, the findings shown in Fig. 4 and 5 indicate that the loss of PERK in HCMV-infected cells promotes the levels of DGs regardless of tail composition.

HCMV infection increases TGs with SFA/MUFA VLCFA tails. Since HCMV infection increases the levels of most TGs, we further characterized the TGs with the greatest relative abundances between infected cells and uninfected cells at 96 hpi. We focused on the top six TGs shown in the heatmap in Fig. 3C. The relative abundance of each of these six TGs was 10- to 18-fold higher in HCMV-infected cells than in uninfected cells at 72 and 96 hpi (Fig. 6A). Each of these TGs had 60 or more total carbons in their tails. TGs have three FA tails, and several molecular forms with different combinations of tails may be present in each of these TGs. The tails in these TGs were identified using MS/MS. At least four tails per TG were identified, demonstrating that each TG represents at least two molecular forms. Furthermore, each TG had at least

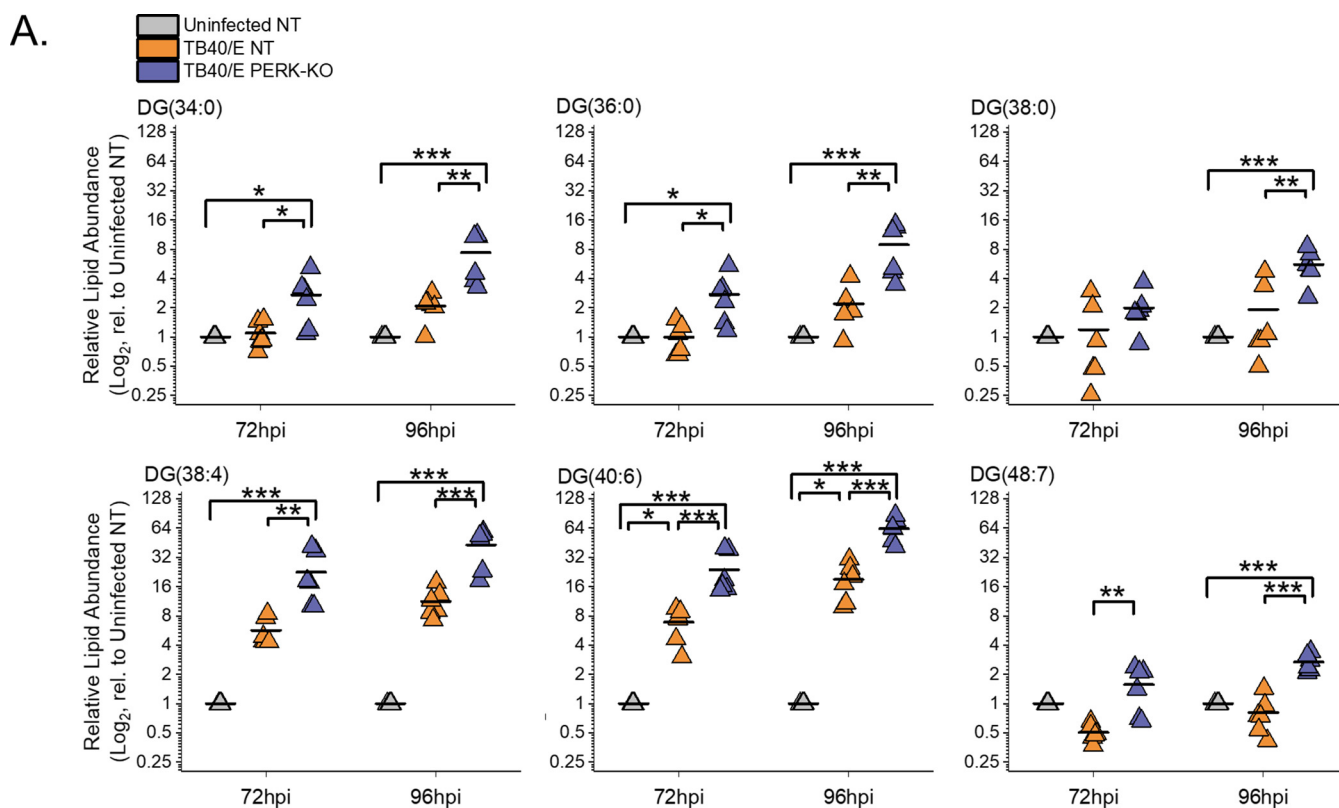


B.

Lipids	Tails	Fold Differences (Relative to uninfected NT)			
		TB40/E NT		TB40/E PERK KO	
		72 hpi	96 hpi	72 hpi	96 hpi
DG(30:1)	C16:1	3.5	18.3	3.8	33.8
DG(36:3)	C16:0, C16:1, C18:1, C18:2, C20:2, C20:3	2.9	8.4	7	14.2
DG(36:4)	C16:0, C18:2, C20:4	10.6	42.4	24.2	91.3
DG(40:3)	C18:0, C22:3	8.3	21.8	9.3	35.5
DG(40:6)	C18:0, C22:6	6.9	19	24	63.3
DG(40:7)	C18:1, C22:6	3.6	21.2	10.1	55.7

FIG 4 HCMV infection elevates DG lipids with long-chain and very-long-chain polyunsaturated fatty acid tails. (A) Levels of DGs that were most prominently changed in TB40/E-infected cells relative (rel.) to those in uninfected cells at 96 hpi. These are the top six elevated DGs shown in the heatmap of Fig. 3C. Three independent experiments were performed, each with duplicated samples, for a total of six data points. Each data point is graphed relative to the levels observed in uninfected NT cells on a log_2 scale. For comparison, the relative levels at 72 hpi are also shown. *, $P < 0.05$; **, $P < 0.01$; ***, $P < 0.001$. One-way ANOVA, Tukey's test. (B) The fatty acid tails for DGs shown in panel A were identified by LC-MS/MS. Long-chain fatty acids (LCFAs) contain 13 to 21 carbons, and very-long-chain fatty acids (VLCFAs) contain 22 carbons or more. LCFAs and VLCFAs that are polyunsaturated fatty acids (PUFAs), i.e., have two or more double bonds, are in bold text. The table contains the average fold changes in abundance of the lipids in TB40/E-infected NT and PERK-KO cells relative to their levels in uninfected NT cells. $n = 6$.

two VLCFA tails with 24 or more carbons ($\geq C_{24}$) (Fig. 6B). Most of the VLCFA tails were SFA (no double bond) or MUFA (a single double bond) tails. In addition to the TGs with SFA and MUFA tails, TG(66:2) and TG(66:3) each had a tail with two double bonds. These results demonstrate that HCMV infection increases the levels of TGs with SFA/MUFA VLCFA tails.



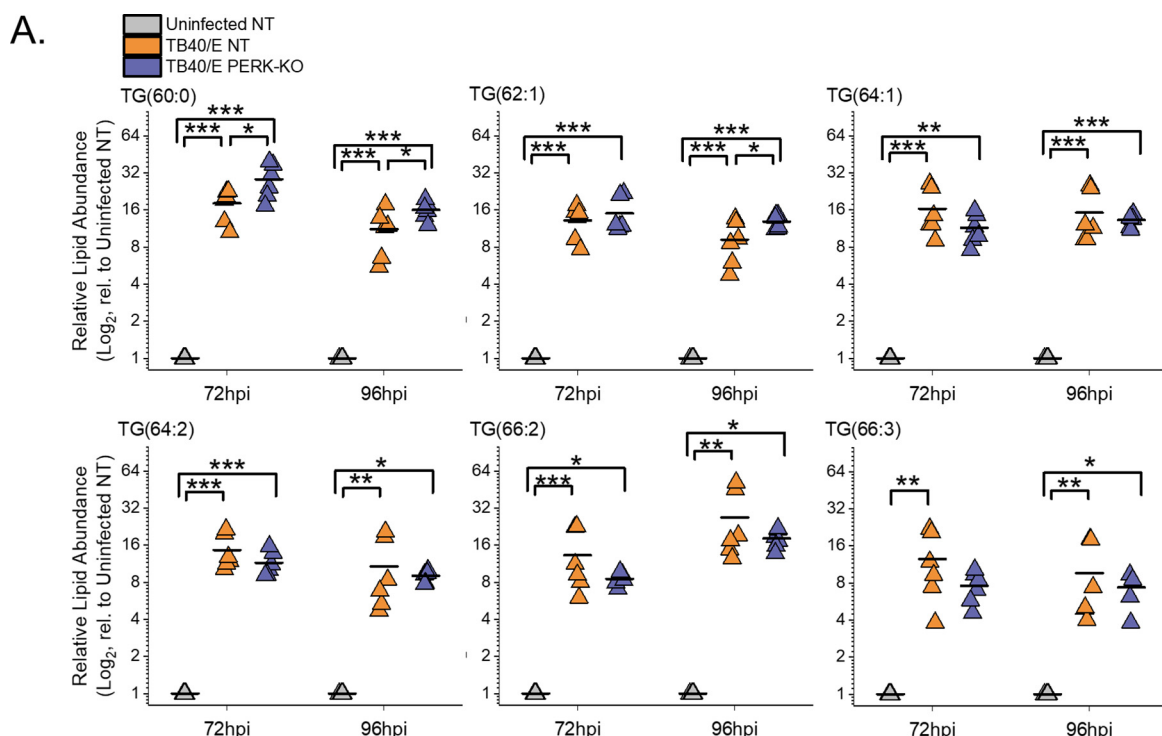
B.

Lipids	Tails	Fold Differences (Relative to uninfected NT)			
		TB40/E NT		TB40/E PERK KO	
		72 hpi	96 hpi	72 hpi	96 hpi
DG(34:0)	C16:0, C18:0	1.1	2.1	2.7	7.4
DG(36:0)	C18:0	1	2.2	2.7	8.9
DG(38:0)	C16:0, C18:0, C20:0	1.2	2	2	5.6
DG(38:4)	C18:0, C18:1, C20:3, C20:4	5.7	10.3	22.5	43.6
DG(40:6)	C18:0, C22:6	6.9	19	23.9	63.3
DG(48:7)	C24:3	0.5	0.8	1.6	2.7

FIG 5 Loss of PERK leads to an accumulation of DGs in HCMV-infected cells. (A) Levels of DGs that were most prominently changed in TB40/E-infected PERK-KO cells relative to levels in infected NT cells at 96 hpi. These represent the top six elevated DGs shown in the heatmap of Fig. 3H. Each data point represents a sample from three independent experiments and is graphed relative to the levels observed in uninfected NT cells on a log_2 scale. For comparison, the relative levels at 72 hpi are also shown. *, $P < 0.05$; **, $P < 0.01$; ***, $P < 0.001$. One-way ANOVA, Tukey's test. (B) The fatty acid tails for DGs shown in panel A were identified by LC-MS/MS. The table contains the average fold changes in abundance of the lipids in TB40/E-infected NT and PERK-KO cells relative to their levels in uninfected NT cells. $n = 6$.

Loss of PERK elevates the levels of TGs with PUFA tails in HCMV-infected cells.

We continued to define the relationship between PERK and the tail composition by examining TGs. Of the six TGs increased the most by HCMV infection, four of the six had levels that were slightly reduced in TB40/E-infected PERK-KO and infected NT cells



B.

Lipids	Tails	Fold Differences (Relative to uninfected NT)			
		TB40/E NT		TB40/E PERK KO	
		72 hpi	96 hpi	72 hpi	96 hpi
TG(60:0)	C16:0, C18:0, C26:0 , C28:0	18.1	11.2	28.3	16
TG(62:1)	C14:0, C16:0, C18:0, C18:1, C20:1, C24:0 , C26:0 , C26:1 , C28:1 , C30:1 , C32:1	13.1	9.2	15	12.9
TG(64:1)	C16:0, C18:0, C18:1, C20:0, C28:0 , C30:1 , C32:1	16.3	15.2	11.4	13.3
TG(64:2)	C16:0, C18:0, C18:1, C20:1, C22:1 , C24:0 , C24:1 , C26:0 , C26:1 , C28:0 , C28:1 , C30:1 , C32:1	14.6	10.7	11.5	9
TG(66:2)	C16:0, C18:1, C24:0 , C24:1 , C28:1 , C30:1 , C32:1 , C34:2 , C34:1	13.3	26.8	8.5	18.1
TG(66:3)	C18:0, C24:1 , C26:1 , C30:1 , C32:2	12.5	9.6	7.6	7.3

FIG 6 HCMV infection increases TGs, including those with saturated and monounsaturated very-long-chain fatty acid tails. (A) Levels of TGs that were most prominently changed in TB40/E-infected cells relative to their levels in uninfected cells at 96 hpi. These are the top six elevated TGs shown in the heatmap of Fig. 3C. Three independent experiments were performed, each with duplicated samples, for a total of six data points. Each data point is graphed relative to the levels observed in uninfected NT cells on a log₂ scale. For comparison, the relative levels at 72 hpi are also shown. *, *P* < 0.5; **, *P* < 0.01; ***, *P* < 0.001. One-way ANOVA, Tukey's test. (B) The fatty acid tails for TGs shown in panel A were identified by LC-MS/MS. Saturated fatty acids (SFAs) contain no double bond, and monounsaturated fatty acids (MUFAs) contain a single double bond in the hydrocarbon tail. VLCFAs that are also SFAs or MUFAs are in bold text. The table contains the average fold change in abundance of the lipids in TB40/E-infected NT and PERK-KO cells relative to their levels in uninfected NT cells. *n* = 6.

(Fig. 6A). These lipids were TG(64:1), TG(64:2), TG(66:2), and TG(66:3). At 72 and 96 hpi, TG(60:0) was more abundant in PERK-KO cells than in NT cells (Fig. 6A). The same is true for TG(62:1) at 96 hpi. These results indicate that, in general, HCMV infection promotes an increase in the abundances of TGs with SFA/MUFA VLCFA tails independently of PERK activity.

Next, we examined the TGs that were altered the most by the loss of PERK in HCMV-infected cells (i.e., the top six TGs in the heatmap shown in Fig. 3H). For each of these six TGs, their levels were 10- to 20-fold higher in TB40/E-infected PERK-KO cells than in infected NT cells at 96 hpi (Fig. 7A). At 72 hpi, most of these TGs were also increased in infected PERK-KO cells relative to levels in infected NT cells. Each of these TGs had at least four tails, demonstrating that all of them have multiple molecular forms (Fig. 7B). Five of the top six TGs contained multiple PUFA tails that were 20 to 26 carbons long (i.e., PUFA VLCFA tails). Levels of none of these TGs were higher in HCMV-infected NT cells than in uninfected NT cells, and some were slightly reduced by infection in NT cells. These observations indicate that in the absence of PERK, HCMV infection increases the levels of TGs with PUFA VLCFAs that are not altered by infection when PERK is present.

In summary, HCMV infection elevates the levels of TGs with SFA/MUFA VLCFAs independently of PERK (Fig. 6). Furthermore, in HCMV-infected cells, the loss of PERK promotes the levels of TGs with PUFA VLCFAs. Together, our observations in Fig. 6 and 7 indicate that in HCMV-infected cells, PERK provides a balance between TGs with SFA/MUFA VLCFA tails and those with PUFA VLCFA tails.

HCMV infection increases the levels of phospholipids (PLs) with SFA/MUFA VLCFA tails. If PERK balances SFA/MUFA and PUFA tails during HCMV infection, we would expect the tails of PLs to also be dysregulated in HCMV-infected PERK-KO cells. We determined whether PERK affects the abundances of PLs following HCMV infection by identifying and measuring their relative concentrations using LC-MS/MS.

First, we determined whether HCMV infection alters the levels of PLs by comparing the relative abundances of PLs in TB40/E-infected cells to those in uninfected cells at 96 hpi. At 96 hpi, 52% of the PLs were upregulated by ≥ 2 -fold in HCMV-infected cells relative to levels in uninfected cells (Fig. 8A and B). In contrast, the levels of only two lipids were downregulated by ≥ 2 -fold after infection (Fig. 8B). Since TB40/E infection increases the levels of PLs at 96 hpi, we examined earlier time points to establish whether TB40/E alters PL levels at 48 and 72 hpi. At 48 hpi, the levels of $\sim 20\%$ of PLs were ≥ 2 -fold higher in HCMV-infected cells than in uninfected cells (Fig. S4A and B). At 72 hpi, 34% of PLs were more abundant (≥ 2 -fold) in infected cells than in uninfected cells (Fig. S4C and D). At 48 and 72 hpi, none of the PLs were reduced by HCMV infection (Fig. S4A to D). These findings show that the levels of several PLs are increased in cells by infection as early as 48 hpi and continue to be elevated at 72 and 96 hpi. Next, we determined whether AD169 infection alters PL levels. At 72 hpi, the levels of several classes of PLs were greater in AD169-infected cells than in uninfected cells (Fig. S4E and F). In both AD169-infected and TB40/E-infected cells, many of the lipids that are elevated the most in infected cells were PLs with SFA/MUFA tails (Fig. 8A and B and Fig. S4). The observations reported here confirm our previous findings that infection with AD169 elevates the abundance of PLs with SFA/MUFA tails, particularly of PLs with SFA/MUFA VLCFAs with 24 or more carbons (8).

We further characterized the PLs with the greatest relative abundances between infected cells and uninfected cells at 96 hpi. We focused on the top six PLs shown in the heatmap in Fig. 8B. The relative abundance of each of these six PLs was 10- to 150-fold higher in HCMV-infected cells than in uninfected cells at 72 and 96 hpi (Fig. 9A). Each of these PLs had 44 or more total carbons in their tails. These PLs had two tails, and several molecular forms with different tail combinations may be present in each. Half of these PLs had only two tails, indicating the presence of a single molecular form. The others represent at least two molecular forms, since we identified at least three tails per PL. Furthermore, each of these PLs contained a SFA or MUFA VLCFA tail with 26 or more carbons (Fig. 9B). These results further demonstrate that HCMV infection increases the levels of PLs with SFA/MUFA VLCFA tails.

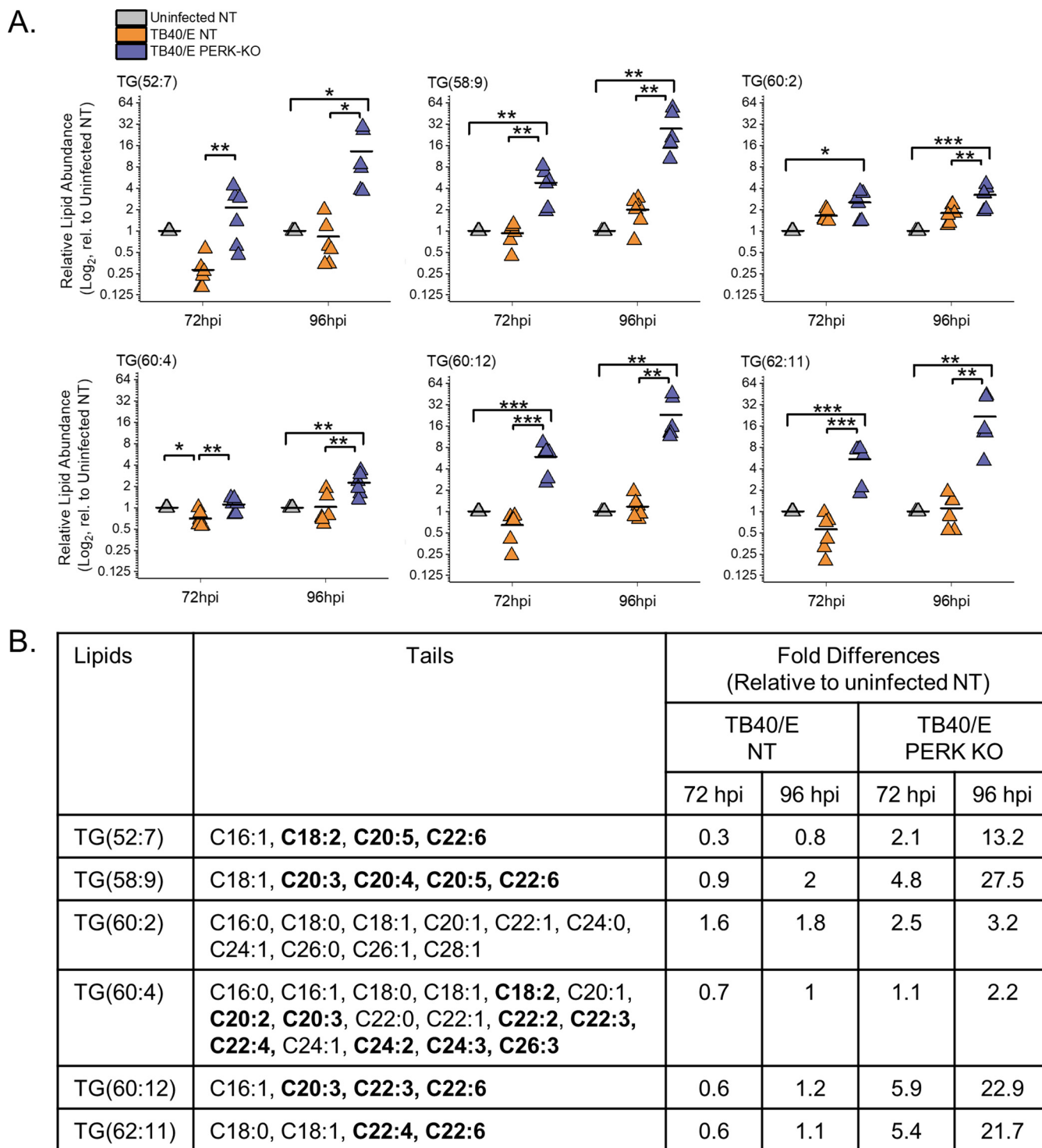


FIG 7 Loss of PERK leads to an accumulation of TGs, including those with PUFA tails, in HCMV-infected cells. (A) Levels of TGs that were most prominently changed in TB40/E-infected PERK-KO cells relative to their levels in infected NT cells at 96 hpi. These represent the top six elevated TGs shown in the heatmap of Fig. 3H. Each data point represents a sample from three independent experiments and is graphed relative to the levels observed in uninfected NT cells on a log₂ scale. For comparison, the relative levels at 72 hpi are also shown. *, $P < 0.5$; **, $P < 0.01$; ***, $P < 0.001$. One-way ANOVA, Tukey's test. (B) The fatty acid tails for TGs shown in panel A were identified by LC-MS/MS. LCFAs and VLCFAs that are PUFAs are in bold text. The table contains the average fold change in abundance of the lipids in TB40/E-infected NT and PERK-KO cells relative to their levels in uninfected NT cells. $n = 6$.

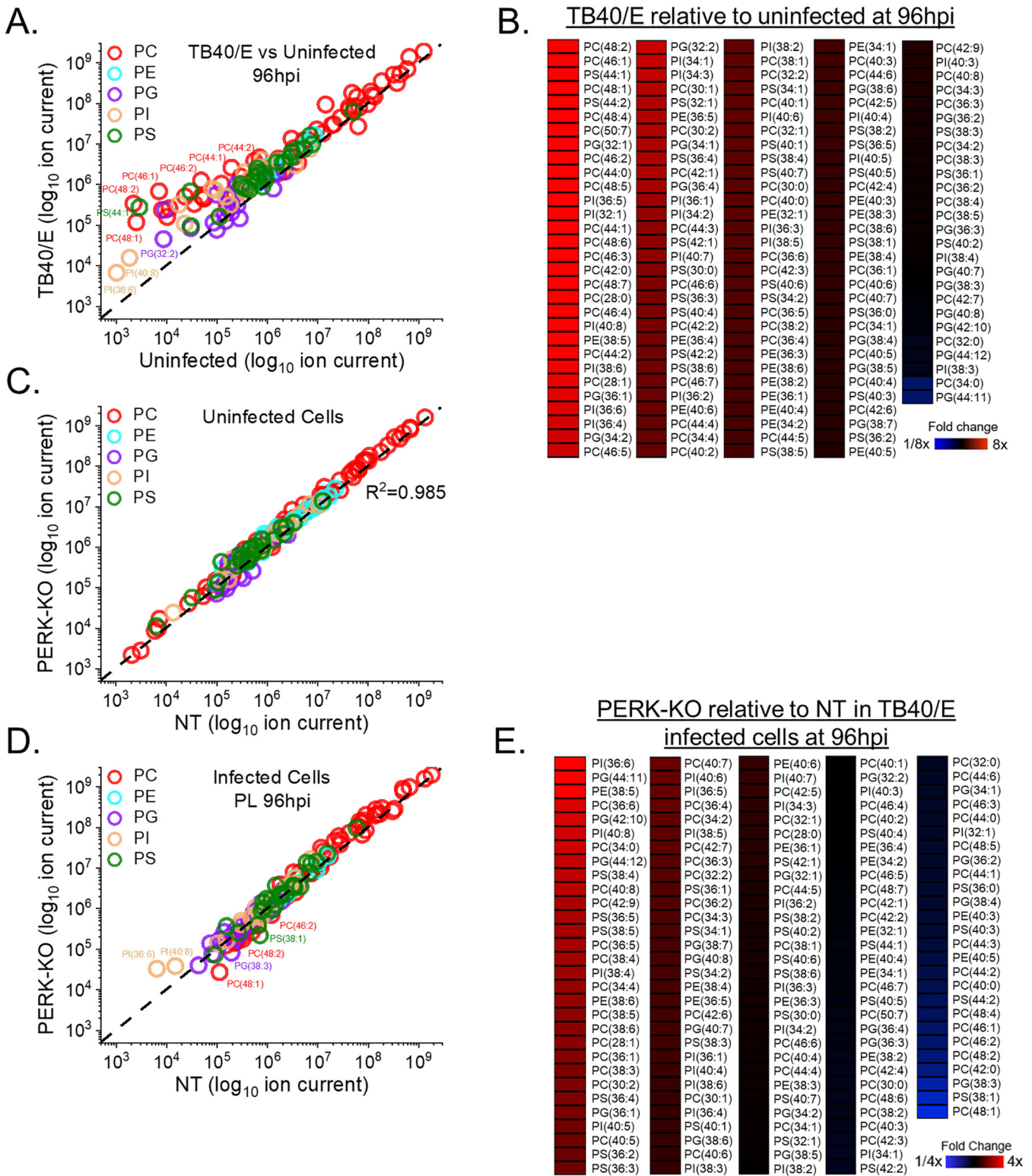
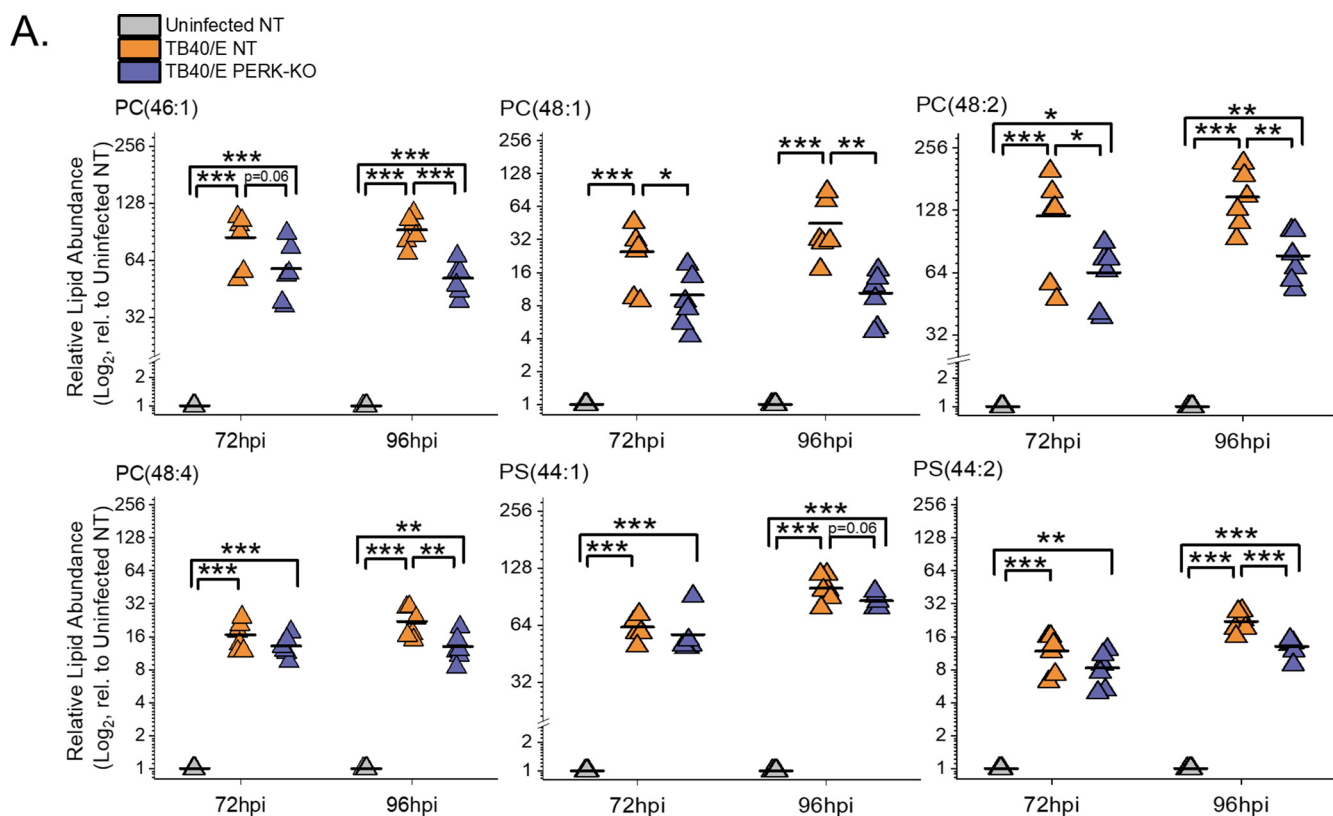


FIG 8 HCMV infection elevates phospholipids (PLs), including some reduced by the loss of PERK. (A, B) Relative levels of PLs in TB40/E-infected and uninfected cells at 96 hpi. PLs were measured by LC-MS/MS following normalization by cell number. Each dot in the plot represents the level of a PL in TB40/E-infected cells relative to its level in uninfected cells. The dashed line represents a relative level of 1 (e.g., the level in infected cells is equal to the level in uninfected cells). (C) Relative levels of PLs in uninfected PERK-KO and NT cells. (D, E) Relative levels of PLs in TB40/E-infected PERK-KO and NT cells at 96 hpi. Abbreviations: PC, phosphatidylcholine; PE, phosphatidylethanolamine; PG, phosphatidylglycerol; PI, phosphatidylinositol; and PS, phosphatidylserine. MOI=3. n=3.



B.

Lipids	Tails	Fold Differences (Relative to uninfected NT)			
		TB40/E NT		TB40/E PERK KO	
		72 hpi	96 hpi	72 hpi	96 hpi
PC(46:1)	C16:0, C18:1, C28:0 , C28:1 , C30:1	85	93	58	52
PC(48:1)	C22:0 , C26:1 , C28:1	25	45	10	10
PC(48:2)	C18:1, C30:1	120	148	64	77
PC(48:4)	C20:3, C20:4, C22:3, C28:1	17	22	13	13
PS(44:1)	C18:1, C26:0	63	100	57	86
PS(44:2)	C18:1, C26:1	12	22	8	13

FIG 9 HCMV infection elevates PLs with SFA and MUFA VLCFA tails that are in part dependent on PERK. (A) Relative abundances of PLs that were most prominently changed in TB40/E-infected cells relative to their levels in uninfected cells at 96 hpi. These are the top six elevated PLs shown in the heatmap of Fig. 8B. Three independent experiments were performed, each with duplicated samples, for a total of six data points. Each data point is graphed relative to the levels observed in uninfected NT cells on a log_2 scale. For comparison, the relative levels at 72 hpi are also shown. *, $P < 0.05$; **, $P < 0.01$; ***, $P < 0.001$. One-way ANOVA, Tukey's test. (B) Tail composition for PLs shown in panel A. Saturated and monounsaturated VLCFAs containing ≥ 22 carbons and one or fewer double bonds are in bold text. The table contains the average fold change in abundance of the lipids in TB40/E-infected NT and PERK-KO cells relative to their levels in uninfected NT cells. $n = 6$.

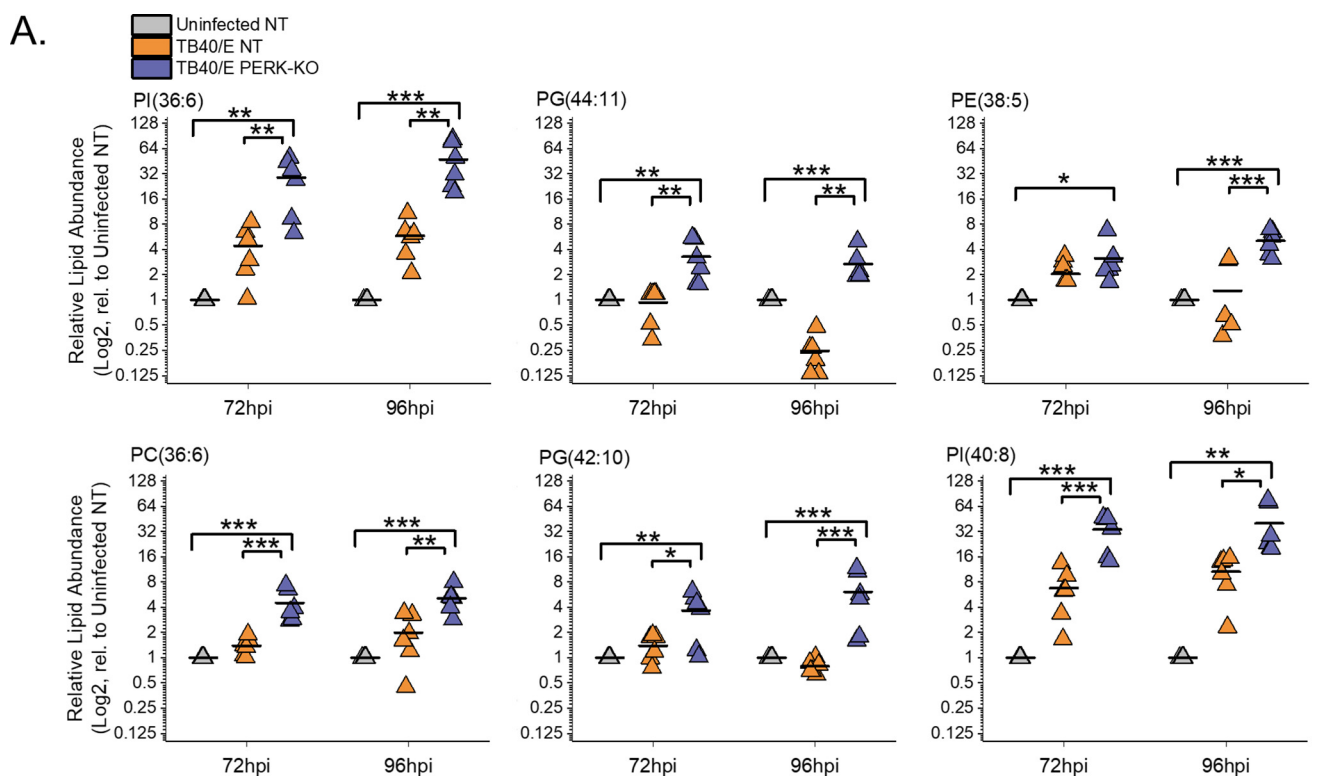
Loss of PERK alters the levels of PLs in HCMV-infected cells. Since the loss of PERK affects the levels of DGs and TGs, we considered whether PERK also affects the levels of PLs in HCMV-infected cells. First, we compared the abundances of PLs in uninfected PERK-KO and NT cells to determine whether PERK regulates the levels of PLs

independently of infection. The levels of PLs in PERK-KO cells are equal to the levels in NT cells, demonstrating that the depletion of PERK has no significant effect on the abundance of PLs in uninfected cells (Fig. 8C). This observation was similar to the DG and TG profile in uninfected PERK-KO and NT cells, providing further evidence to support the idea that PERK does not regulate lipid metabolism in uninfected cells under the conditions used in our experiments.

Next, we examined whether the loss of PERK affects PL levels in HCMV-infected cells. We infected PERK-KO and NT control cells with TB40/E at an MOI of 3. At 96 hpi, the levels of several PLs were greater in HCMV-infected PERK-KO cells than in infected NT cells (Fig. 8D and E). We found that ~16% of PLs were ≥ 2 -fold more abundant in HCMV-infected PERK-KO cells than in infected NT cells (Fig. 8D and E). Many of the PLs elevated in TB40/E-infected PERK-KO cells at 96 hpi were also elevated at 72 hpi (Fig. S5A and B). Next, we determined whether PERK was required for changes in PL levels following infection with AD169. As with TB40/E-infected PERK-KO cells, the levels of several PLs in AD169-infected PERK-KO cells were greater than in infected NT cells (Fig. S5C and D).

Loss of PERK reduces the levels of PLs with SFA/MUFA VLCFA tails. Some PL levels were reduced in HCMV-infected PERK-KO cells. Approximately 6 to 12% of PLs in TB40/E- and AD169-infected PERK-KO cells were reduced by ≥ 2 -fold compared to levels in infected NT cells (Fig. 8D and E and Fig. S5). The levels of several of these PLs are increased by HCMV infection in NT cells but reduced by the loss of PERK, suggesting that PERK supports HCMV-induced increases in the relative abundance of PLs. To further investigate this possibility, we focused on the PLs that were elevated the most in TB40/E-infected cells relative to levels in uninfected cells at 96 hpi (i.e., the lipids shown in Fig. 8B). Of the six PLs elevated the most by HCMV infection, most were reduced in infected PERK-KO cells relative to levels in infected NT cells (Fig. 9A). For example, phosphatidylcholine 48:2 [PC(48:2)] was the PL with the highest level of increase in TB40/E-infected cells relative to its levels in uninfected cells at 48, 72, and 96 hpi (Fig. 8A and B, 9A, and Fig. S4A to D). PC(48:2) was also among the PLs exhibiting the largest changes following AD169 infection (Fig. S4E and F). However, in TB40/E-infected or AD169-infected PERK-KO cells, the level of PC(48:2) was significantly reduced relative to its level in infected NT cells (Fig. 8D and E and 9A and Fig. S5). These findings suggest that PERK promotes the levels of PLs with SFA/MUFA VLCFA tails in HCMV-infected cells. While the levels of these lipids are lower in HCMV-infected PERK-KO than in infected NT cells, their levels in infected PERK-KO cells are still higher than in uninfected cells (Fig. 9A). For example, PC(48:2) is >50 -fold more abundant in TB40/E-infected PERK-KO cells than in uninfected cells (Fig. 9A). This observation suggests that PERK is not required to induce changes in lipid levels following HCMV infection but may be necessary to promote specific changes in the lipidome. Overall, we conclude that PERK helps promote the levels of PLs with SFA/MUFA VLCFA tails in HCMV-infected cells.

Loss of PERK elevates the levels of PLs with PUFA tails. We sought to understand further the role of PERK in regulating PL levels in HCMV-infected cells by identifying the lipids that were increased the most by the loss of PERK in HCMV-infected cells (i.e., the top six PLs in the heatmap shown in Fig. 8E). For each of these six PLs, their levels were >2.5 -fold higher in TB40/E-infected PERK-KO cells than in infected NT cells at 96 hpi (Fig. 10A). At 72 hpi, most of these PLs were also increased in infected PERK-KO cells relative to levels in infected NT cells. These lipids were 3- to 45-fold more abundant in HCMV-infected PERK-KO cells than in uninfected NT cells. However, their levels were similar in HCMV-infected NT cells and uninfected NT cells, demonstrating that HCMV infection does not significantly alter their abundance when PERK is present (Fig. 10A). These PLs were phosphatidylinositol (PI), phosphatidylglycerol (PG), phosphatidylethanolamine (PE), and PC lipids. We identified tails for four of these lipids but were unable to identify the tails for the PI lipids using our MS/MS approach. These PLs contained PUFA tails ranging in length from 20 to 22 carbons (Fig. 10B). Based on the



B.

Lipids	Tails	Fold Differences (Relative to uninfected NT)			
		TB40/E NT		TB40/E PERK KO	
		72 hpi	96 hpi	72 hpi	96 hpi
PI(36:6)	N.D.	4	6	29	47
PG(44:11)	C18:0, C22:5 , C22:6	1	0.2	3	3
PE(38:5)	C16:0, C18:0, C18:1, C20:4 , C20:5 , C22:5	2	1	3	5
PC(36:6)	C16:1, C20:5 , C22:6	1	2	5	5
PG(42:10)	C18:0, C20:4 , C22:6	1	1	4	6
PI(40:8)	N.D.	7	11	34	40

FIG 10 Loss of PERK leads to an accumulation of PLs with PUFA tails in HCMV-infected cells. (A) Abundances of PLs that were most prominently changed in TB40/E-infected PERK-KO cells relative to their levels in infected NT cells at 96 hpi. These are the top six elevated PLs shown in the heatmap of Fig. 8E. Each data point is graphed relative to the levels observed in uninfected NT cells on a log₂ scale. For comparison, the relative levels at 72 hpi are also shown. *, $P < 0.05$; **, $P < 0.01$; ***, $P < 0.001$. One-way ANOVA, Tukey's test. (B) Tail compositions for PLs shown in panel A. LCFAs and VLCFAs that are polyunsaturated are in bold text. The table contains the average fold change in abundance of the lipids in TB40/E-infected NT and PERK-KO cells relative to their levels in uninfected NT cells. ND, not determined. $n = 6$.

observations shown in Fig. 10, we conclude that the loss of PERK promotes the levels of PLs with PUFA tails in HCMV-infected cells.

PERK enhances ELOVL7 protein levels but not ELOVL5 levels. The lipid analysis demonstrated that PERK regulates a balance between SFA/MUFA VLCFA tails and PUFA tails in TGs and PLs in HCMV-infected cells. ELOVL7 elongates SFA and MUFA

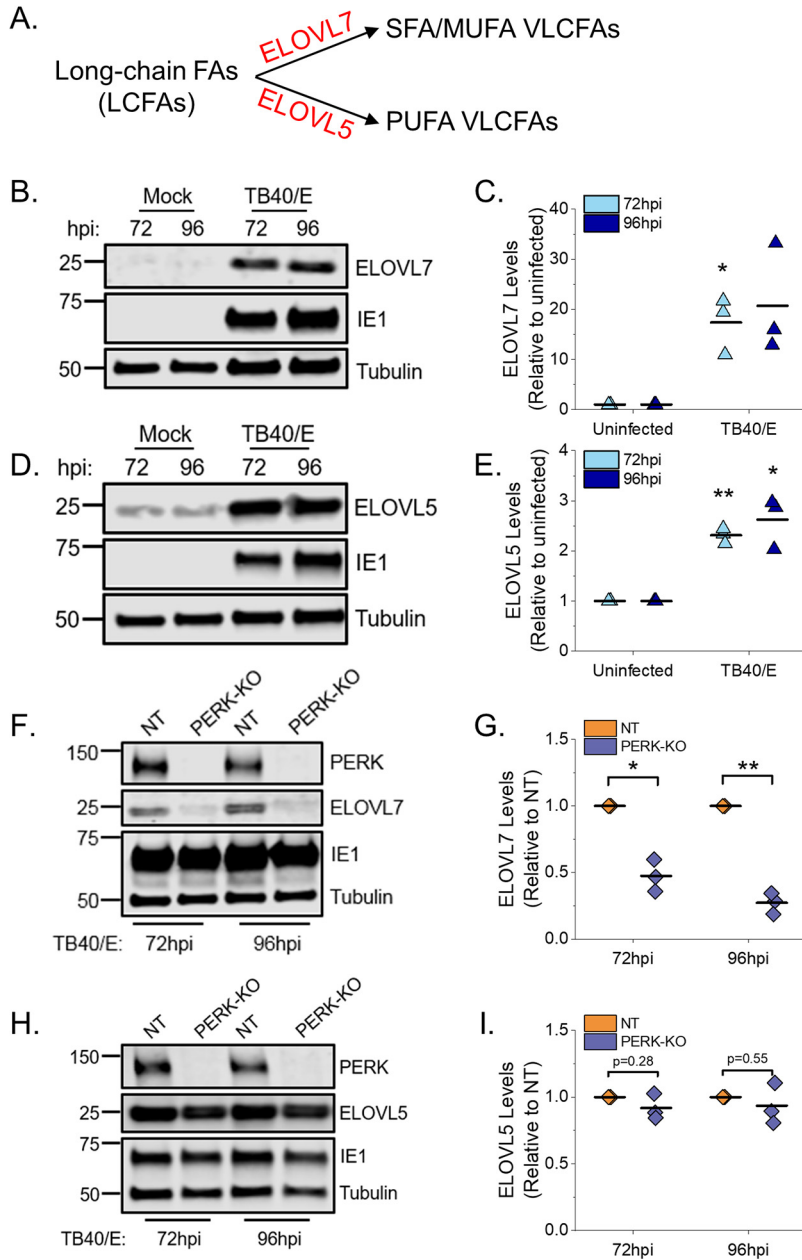


FIG 11 PERK enhances the protein levels of ELOVL7 but not ELOVL5. (A) Schematic showing ELOVL7 and ELOVL5 elongation of SFA/MUFA VLCFAs and PUFA VLCFAs, respectively. (B, C) Western blot analysis and protein quantification for ELOVL7 in HCMV-infected and uninfected HFF cells. ELOVL7 protein levels were normalized to tubulin. (D, E) Western blot analysis and protein quantification for ELOVL5 in HCMV-infected and uninfected HFF cells. (F, G) Western blot analysis and protein quantification for ELOVL7 in TB40/E-infected PERK-KO and NT cells. (H, I) Western blot analysis and protein quantification for ELOVL5 in TB40/E-infected PERK-KO-c1 and NT cells. *, $P < 0.05$; **, $P < 0.01$. One-sample t test. MOI of 1. $n = 3$.

VLCFAs (Fig. 11A) (13, 15, 16, 27). ELOVL7 is also required for HCMV replication (13). We previously demonstrated that HCMV infection with AD169 increases ELOVL7 gene expression and that protein levels start to increase by 48 hpi and remain elevated from 72 to 120 hpi (13). First, we determined whether infection with TB40/E increases ELOVL7 with similar kinetics. In NT cells infected with TB40/E at an MOI of 1, the level of ELOVL7 increases as replication progresses and is maximally expressed at 72 to 96 hpi (Fig. S6). Next, we confirmed whether TB40/E infection increases ELOVL7 protein

levels at 72 and 96 hpi in HFF cells that have not been genetically modified by CRISPR/Cas9 or any other means. Protein levels of ELOVL7 were also upregulated by 17- to 20-fold in HCMV-infected HFF cells compared to levels in uninfected cells at 72 and 96 hpi, respectively (Fig. 11B and C). HCMV replication relies on ELOVL5, in addition to ELOVL7 (13). ELOVL5 elongates PUFA VLCFAs (Fig. 11A) (15, 19). HCMV infection also increases ELOVL5 gene expression (13) and protein levels by 2.5-fold at 72 and 96 hpi in HFF cells (Fig. 11D and E). We hypothesized that during HCMV replication, PERK balances SFAs/MUFAs and PUFAs by regulating ELOVL7 and ELOVL5 protein levels. To test our hypothesis, we infected PERK-KO and NT control cells with TB40/E and measured the protein levels of ELOVL7 and ELOVL5. From 4 to 48 hpi, the levels of ELOVL7 were low and reduced in TB40/E-infected PERK-KO cells relative to levels in infected NT cells (Fig. S6). At 72 and 96 hpi, the levels of ELOVL7 continued to remain low and were >2-fold lower in HCMV-infected PERK-KO cells than in infected NT cells (Fig. 11F and G and Fig. S6). However, the levels of ELOVL5 in HCMV-infected PERK-KO and NT cells were similar at 72 and 96 hpi (Fig. 11H and I). We conclude that PERK is necessary for HCMV infection-related increases in ELOVL7, but not ELOVL5, protein levels.

DISCUSSION

Metabolic reprogramming by HCMV requires several host factors, including those associated with cellular stress responses (4, 28–31). While both HCMV infection and ER stress are known to regulate lipid metabolism (3, 7, 8, 10, 12, 13, 32, 33), the role of ER stress in HCMV reprogramming of lipid synthesis is poorly defined. The increase in lipid metabolism following HCMV infection depends on several host factors, including the ER stress-related kinase PERK (7). However, the effects of PERK on the metabolism of specific classes or types of lipids are unknown. In this study, we used CRISPR/Cas9 engineering, virus replication assays, and lipidomics to define how PERK regulates lipid levels in HCMV-infected cells.

HCMV infection increases PERK protein levels and activity, as measured by autophosphorylation and ATF4 protein levels (5, 21, 22). Here, we show that TB40/E infection increases ATF4 protein levels by 48 to 120 hpi via a PERK-dependent mechanism (Fig. 1 and 2). We find that infection increases ELOVL7 protein levels by a PERK-dependent mechanism with kinetics similar to those of ATF4 expression (Fig. 11 and Fig. S6). Many of the mechanisms used by HCMV to induce host stress responses, including PERK, are unknown. The viral ER-resident glycoprotein pUL148 activates PERK (5) and reorganizes the ER membrane (6). However, infection with AD169, which lacks the *UL148* gene, promotes PERK, indicating that HCMV encodes multiple mechanisms to activate PERK (8). Another HCMV protein, pUL37x1, induces the release of Ca²⁺ from the ER into the cytosol (34), which may potentially cause ER stress (3, 35). We found that pUL37x1 promotes PERK and ELOVL7 protein levels (8). PL VLCFAs with SFA/MUFA tails are reduced in cells infected with a mutant virus that lacks the *UL37x1* gene (8), further suggesting that Ca²⁺ flux may be a mechanism involved in inducing ER stress and remodeling of the host lipidome following HCMV infection. Another viral protein, pUL38, that activates PERK (22) also promotes ELOVL7 expression (13), providing further evidence of a connection between PERK and FA elongation. These observations suggest that HCMV encodes several mechanisms to activate ER stress, each of which may contribute to the reprogramming of lipid metabolism following infection.

HCMV infection increases the flow of carbons from nutrients to lipid synthesis. Carbons from glucose and acetate are used to generate FAs, including VLCFAs made by ELOVLs (8, 12, 13, 26). Using AD169, we previously demonstrated that HCMV infection increases ELOVL5 and ELOVL7 transcripts, ELOVL7 protein levels, FA elongation, VLCFA synthesis, the abundance of PLs with SFA/MUFA tails, and the levels of PERK protein (8, 13, 14). The current study confirms that HCMV infection increases FA elongation, VLCFA synthesis, the abundance of PLs with SFA/MUFA VLCFA tails, and PERK protein level and activity using the low-passage-number TB40/E strain. Moreover, HCMV infection increases the cellular abundance of most DGs and TGs with SFA/MUFA

VLCFA tails (Fig. 3A to C). Using CRISPR/Cas9-engineered PERK-KO cells, we demonstrate that PERK contributes to the regulation of lipid levels in HCMV-infected cells. In PERK-KO cells, the levels of DGs, TGs, and PLs with PUFA tails rise following HCMV infection (Fig. 3F to H, 4, 5, 7, 8D and E, and 10). PUFA tails are elongated by ELOVL5 (15, 19). HCMV-infected cells have a higher level of ELOVL5 protein than uninfected cells (Fig. 11D and E). ELOVL5 protein levels increase following HCMV infection independently of PERK (Fig. 11H and I), consistent with an increase in lipids with PUFA tails in infected PERK-KO cells. In HCMV-infected PERK-KO cells, the levels of PLs with SFA/MUFA VLCFA tails are reduced relative to those in infected NT control cells (Fig. 8D and E and 9A and B), suggesting that PERK promotes the synthesis of PLs with SFA/MUFA VLCFA tails, which can be synthesized by ELOVL7 (13, 15, 16, 27). ELOVL7 promotes HCMV replication by supporting the release of infectious virions (13). In this study, we find that PERK is necessary for efficient replication of HCMV (Fig. 2C and D and Fig. S1D and E), at least in part, by promoting the infectivity of released virus particles and cell-to-cell spread (Fig. 2E and Fig. S1D). Moreover, PERK helps promote levels of ELOVL7 protein and PLs with SFA/MUFA VLCFA tails in HCMV-infected cells (Fig. 8 and 11). Further, the loss of PERK reduces the particle-to-infectious virion ratio (Fig. 2E), as is the case when ELOVL7 is depleted (13). Our observations collectively show that the regulation of lipid metabolism and virus replication in HCMV-infected cells involves a PERK-dependent mechanism.

In HCMV-infected PERK-KO cells, ELOVL7 levels are significantly reduced, but not ELOVL5 protein levels (Fig. 11). This loss in the balance of ELOVL5 and ELOVL7 proteins likely reduces the available pool of SFA/MUFA VLCFAs relative to the pool of PUFA VLCFAs. This shift in the saturation status in the pool of available FA tails may explain why lipids with PUFA tails increase in PERK-KO cells (Fig. 3D to H). Based on our observations, we propose a model wherein PERK, through ELOVL7 activity, promotes the synthesis of SFA/MUFA VLCFAs (Fig. 12). This action balances the elongation of PUFAs made by ELOVL5, which HCMV infection promotes through an unknown PERK-independent mechanism. The pool of SFA/MUFAs and PUFAs is used to synthesize lipids, resulting in DGs with SFA/MUFA or PUFA tails. At this point, DGs can be further metabolized to generate PLs or TGs. HCMV infection promotes the synthesis of PLs and TGs from DG-SFAs/MUFAs. We further propose that the synthesis of PLs with SFA/MUFA VLCFA tails supports the release of infectious virions. This idea is further supported by the observation that the virus envelope of HCMV is enriched with PLs with SFA/MUFA VLCFA tails (13, 36). Moreover, the kinetics of the lipid changes that we observed following HCMV infection further support this model. Infection promotes PERK activity—as measured by ATF4 levels—maximally at 48 to 96 hpi (Fig. 1). Similarly, HCMV infection increases ELOVL7 at 48 to 96 hpi, and lipid changes, including the increases in DG, TG, and PL lipids, occur as early as 48 hpi and continue to be promoted through 96 hpi (Fig. 3 and 10 and Fig. S2 to S4). We observed maximal lipid changes at 72 and 96 hpi, when cells are producing new viral progeny.

Furthermore, we find that, in general, PERK supports an increase in PLs with SFA/MUFA VLCFA tails following HCMV infection but not necessarily TGs with SFA/MUFA VLCFAs (compare Fig. 9 to Fig. 6). This observation may indicate that in addition to regulating ELOVLs, PERK may promote the flow of DGs to PLs rather than to TGs (Fig. 12). HCMV infection may enhance TG synthesis through a PERK-independent mechanism. PERK may affect the flow of lipids through the synthesis pathway by acting directly on the lipid head group. PERK has been reported to phosphorylate DG to generate phosphatidic acid (PA) (23). Since PA lipids are upstream of DGs in the TG and PL synthesis pathways, DG conversion to PA by PERK would reduce the synthesis of TGs and PLs. Since the levels of TGs and PLs were increased in HCMV-infected cells, it seems unlikely that PERK phosphorylates DGs during virus replication. Nevertheless, at this stage, we cannot rule out the possibility that PERK promotes the flow of DGs to PLs, either directly or indirectly.

While HCMV replication depends on ELOVL7 activity, the overproduction of saturated VLCFAs by ELOVL7 is cytotoxic (37). Necroptotic cells have increased abundances of PC,

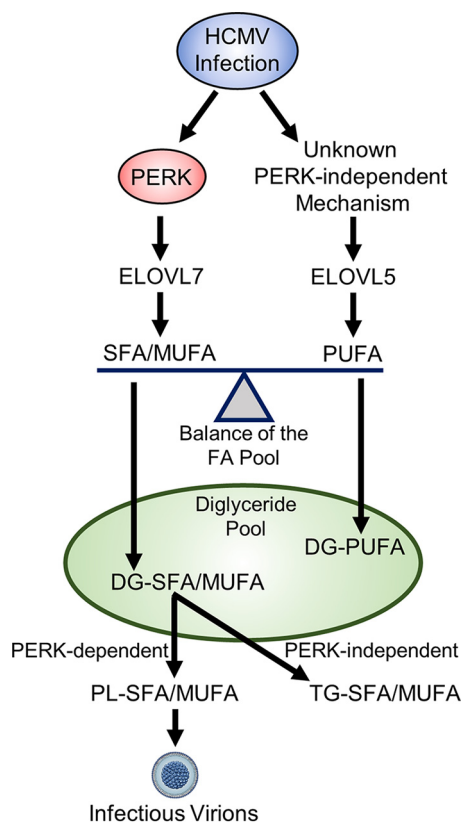


FIG 12 Model for PERK balancing of lipids with SFA/MUFA and PUFA tails through ELOVL7. HCMV infection increases the elongation of FAs by promoting ELOVL5 and ELOVL7. In HCMV-infected cells, PERK activity promotes ELOVL7, increasing the synthesis of SFAs and MUFAs. HCMV infection also increases ELOVL5 through an unknown PERK-independent mechanism. ELOVL5 elongates PUFAs. Both SFAs/MUFAs and PUFAs are incorporated into lipids through synthesis pathways, generating a pool of DGs with SFA/MUFA or PUFA tails. The role of DG-PUFAs in HCMV replication is currently unknown. In HCMV-infected cells, PERK further promotes lipid synthesis by directing DG-SFAs/MUFAs toward PL synthesis pathways, generating PL-SFAs/MUFAs. PLs with SFA/MUFA tails are used to generate infectious virions. HCMV infection also promotes the synthesis of TG-SFAs/MUFAs from DG-SFAs/MUFAs through an unknown PERK-independent mechanism. The role of TG-SFAs/MUFAs in HCMV replication is currently unknown.

DG, and TG lipids with SFA/MUFA VLCFA tails (38). An increase in lipotoxicity may reduce viral replication if cell death occurs before the production of viral progeny. To overcome cell death associated with viral infection, HCMV encodes several inhibitors of cell death pathways (39, 40). The relationship between ER stress and lipid metabolism is bidirectional: ER stress regulates lipid metabolism, and lipids can induce ER stress. An overabundance of SFAs induces ER stress, which can be mollified by PUFAs (41–44). It is possible that HCMV-infected cells maintain a balance between PUFAs and SFA/MUFAs to limit lipotoxic stress. If this is the case, then balancing the lipid products of ELOVL5 and ELOVL7 would support HCMV replication. Currently, the importance of ELOVL5 and lipids with PUFA tails in HCMV replication is unknown and is of interest for further study.

PERK can regulate FA synthesis by inducing the maturation of sterol regulatory-element binding proteins (SREBPs) (7). SREBPs are transcription factors that promote the expression of lipogenic genes, including ELOVLs. However, overexpression of SREBP1 in PERK knockdown cells only partially rescued the loss in lipid synthesis, suggesting that PERK uses additional mechanisms to regulate lipid metabolism (7). Moreover, PERK promotes the transcriptional activity of ATF4, a transcription factor that controls amino acid and lipid metabolism during stress (45–50). In white adipose tissue in mice, ATF4 upregulates the expression of FA synthase (FAS) and stearoyl coenzyme A (stearoyl-CoA) desaturase-1 (SCD1) (48). In HCMV-infected cells, PERK activity increases ATF4

protein levels (Fig. 2) (5, 21, 22), allowing for a possible role of ATF4 in HCMV-induced lipogenesis. If ATF4 acts downstream of PERK to regulate lipid metabolism, it may contribute to balancing the pool of SFAs/MUFAs and PUFAs. While continued work is necessary to further define the mechanistic details of PERK's regulation of lipid metabolism, our findings demonstrate a previously unknown role of PERK differentially regulating the activities of ELOVLs.

Humans encode seven ELOVLs (ELOVL1 to 7). While gene expression of all ELOVLs is known to be differentially regulated in a tissue- and cell type-dependent manner (15), the mechanisms that differentially regulate them are undefined. Our observation that ELOVL5 and ELOVL7 protein levels are differentially regulated by a PERK-dependent mechanism (Fig. 11) provides insight into the cellular control of ELOVLs. Importantly, the observations reported in this study suggest that the differential control of ELOVLs is regulated by a stress response induced by viral infection. It may be possible that stress induced by nonviral triggers will similarly lead to the differential regulation of ELOVLs. It is noteworthy that the loss of PERK had minimal effect on the levels of lipids in uninfected cells (Fig. 3D and E and Fig. 8C). It is possible that this is due to a lack of stress stimuli in our uninfected cells, and PERK-dependent lipidome changes may occur in uninfected cells following activation of ER stress. Outside the context of infection, ELOVL7 is expressed in many tissues, with the highest levels in the pancreas and prostate (15, 16), and its overexpression is associated with prostate cancer (16). ELOVL7 is also expressed in the brain, and a decrease in its expression correlates with Parkinson's disease (51). It is unknown whether a PERK-dependent mechanism controls ELOVL7 protein levels in these diseases. Nonetheless, our finding that PERK differentially regulates ELOVLs to promote ELOVL7 highlights the need for continued studies to understand the role of ER stress in regulating lipid metabolism in viral and nonviral diseases.

While the complex interactions between ER stress and lipid metabolism remain incompletely understood, the conclusions provided in this report highlight that HCMV replication relies on the regulation of lipid metabolism by a stress response to promote FA elongation and to control the relative levels of lipids in host cells. Following HCMV infection, PERK regulates lipid metabolism by promoting ELOVL7, but not ELOVL5. ELOVL7 supports the infectivity of released HCMV virions, and its SFA VLCFA products are present in the HCMV envelope (13). By regulating ELOVL7 and lipid metabolism, PERK—and more broadly, ER stress—may be necessary for the membrane biogenesis needed for HCMV replication. Overall, this study furthers our understanding of the mechanisms by which HCMV induces lipogenesis to ensure virus replication by demonstrating that PERK is an essential factor in HCMV-host metabolism interactions.

MATERIALS AND METHODS

Cells and viruses. Human foreskin fibroblast (HFF) cells were cultured in Dulbecco's modified Eagle's medium (DMEM) containing 10% fetal bovine serum (FBS), 10 mM HEPES, and penicillin-streptomycin. Prior to infection, cells were maintained at full confluence for 3 days in serum-containing growth medium. Cells were switched to serum-free medium (DMEM, HEPES, and penicillin-streptomycin) the day before infection. HCMV AD169 and green fluorescent protein (GFP) expressing TB40/E strains were used throughout the study (8, 52–54). Cells were infected at a multiplicity of infection (MOI) of 1 or 3 infectious units per cell, depending on the experiment. Uninfected cells were mock infected by treating the cells the same as infected cells, with the exception that the inoculum lacked virus particles. At 48 hpi, the growth medium was replaced with fresh media to maintain nutrient levels. All virus stocks were made by pelleting virus from the supernatant of infected cells through 20% sorbitol using ultracentrifugation. Viruses were resuspended in serum-free DMEM and stored at -80°C . Infectious virus titers were measured by determining the 50% tissue culture infectious dose (TCID_{50}). The particle-to-infectious unit ratio was determined by calculating the ratio between viral DNA and infectious virus yield in cell-free supernatants. The determination of virus yields from cell-free supernatants is described elsewhere (55). Viral DNA in supernatants was quantified by quantitative PCR (qPCR) as previously described (56).

Generation of PERK knockout cells using CRISPR/Cas9 engineering. Single guide RNA (sgRNA) sequence specific for the human PERK gene was cloned into LentiCRISPR-v2 (57, 58), which coexpresses a mammalian codon-optimized Cas9 nuclease and a sgRNA (26). A sgRNA that does not target any human or HCMV sequence was used for a nontargeting (NT) control. The gRNA sequences used in CRISPR knockout experiments are as follows: PERK-KO-c1, CACCTCAGCGACGCGAGTAC; PERK-KO-c2, TGGAGCGCGCCATCAGCCCG; and NT, CGTTCCGCGCCCGTTCAA. Lentiviruses containing Cas9 and sgRNA were produced in 293T cells and transduced into life-extended primary HFFs (HFF-human

telomerase reverse transcriptase [hTERT]), followed by drug selection using 2 μ g/ml puromycin. Single-cell clones were obtained by dilution into a 96-well plate by seeding 1.5 transduced cells plus 200 non-transduced HFFs, as previously described (26). CRISPR-treated cells were selected a second time using 2 μ g/ml puromycin once the cells reached 85 to 90% confluence. PERK knockout was confirmed by Western blotting and sequencing using the Guide-IT indel kit (TaKaRa Bio) and primers targeting the corresponding genomic region of the PERK gene. Each clone was sequenced at least 20 times to ensure biallelic mutations in the PERK gene. In parallel, the PERK gene was sequenced in the NT cells to confirm that the HFF-hTERT cells used contained a wild-type PERK gene.

Focus expansion assay measuring cell-to-cell spread of HCMV infection. Cell-to-cell spread was measured by immunofluorescence detection under microscopy as previously described (59, 60). Briefly, 150,000 cells per well of PERK-KO or NT control cells were seeded in a 12-well plate and grown to full confluence for 3 days. Cells were infected with TB40/E HCMV for 24 h. At 24 hpi, cells were overlaid with growth media with methylcellulose for another 8 days. At 5 dpi, fresh media with methylcellulose were added to cells. At 9 dpi, cells were fixed with 4% paraformaldehyde (PFA) for 10 min at 4°C. HCMV-infected cells were stained with mouse monoclonal anti-IE1 (clone 63-27) and mouse monoclonal anti-pp65 (clone 28-277) and detected by immunofluorescence microscopy. The images were acquired by an Axio-Observer.Z1 fluorescence microscope and the AxioVision 4.8 software.

Lipidomics. The abundance of lipids was measured using liquid chromatography–high-resolution tandem mass spectrometry (LC-MS/MS) as previously described (8). Briefly, cells were washed with PBS and lysed in cold 50% methanol. Lipids were extracted twice using chloroform and dried under nitrogen gas. Lipids then were resuspended in 100 μ l of a 1:1:1 solution of methanol-chloroform-isopropanol per 200,000 cells. For each sample, a total of three wells were used for analysis. Two wells were used for lipid extraction (i.e., duplicate samples analyzed in parallel to determine technical variation), and one well was used to determine the total number of cells. Samples were normalized according to the number of live cells at the time of lipid extraction. A fourth well with no cells was used as a control to determine any contaminants from the lipid extraction and LC-MS/MS steps. Any mass spectral feature from this contaminant list that appeared in the samples was removed from the analysis. During data collection, the samples were stored at 4°C in an autosampler.

Splash Lipidomix lipidomic mass spectrometry standards (Avanti polar lipids) were used in determining extraction efficiencies and lipid quantitation. Following resuspension, lipids were stored at 4°C in an autosampler. Lipids were separated by reverse-phase chromatography using a Kinetex 2.6- μ m C₁₈ column (Phenomenex; 00F-4462-AN). LC was performed at 60°C using a Vanquish ultrahigh-performance LC (UHPLC) system (Thermo Scientific) and two solvents: solvent A (40:60 water-methanol plus 10 mM ammonium formate and 0.1% formic acid) and solvent B (10:90 methanol-isopropanol plus 10 mM ammonium formate and 0.1% formic acid). UHPLC was performed at a 0.25-ml/min flow rate, starting at 25% solvent B and ending at 100% solvent B as described previously (8). After each sample, the column was washed and equilibrated. The total run time was 30 min per sample. Blank samples were run before, after, and at the same time as (interspersed with) the samples. Lipids were measured using a Q-Exactive Plus mass spectrometer operating in a full MS/data-dependent MS2 (dd-MS2) TopN mode. MS1 data were collected at a resolution of either 70,000 or 140,000. Additional settings were as follows: an automatic gain control (AGC) target of 1e6, transient times of 250 ms for a 70,000 resolution, and 520 ms for a 140,000 resolution. MS1 spectra were collected over a mass range of 200 to 1,600 *m/z*. MS2 spectra were collected using a transient time of 120 ms and a resolution setting of 35,000 with an AGC target of 1e5. Each sample was analyzed using negative and positive ion modes. The mass analyzer was calibrated weekly. Lipids were ionized using a heated electrospray ionization (HESI) source and nitrogen gas as described previously (8). Lipids were identified and quantified using MAVEN (61), EI-MAVEN (Elucidata), and Xcalibur (Thermo Scientific) as previously described (8).

Protein analysis. Proteins were examined by Western blotting using SDS-PAGE performed with Tris-glycine-SDS running buffer. Proteins were separated using Mini-Protean TGX Any kD or 4% to 20% gels (Bio-Rad) and transferred to an Odyssey nitrocellulose membrane (LI-COR). Membranes were blocked using 5% milk in Tris-buffered saline with 0.05% Tween 20 (TBS-T) and incubated with primary antibodies in the presences of 1% milk–TBS-T solution, except for anti-ATF4 and anti-pUL123, which were incubated in the presence of 3% and 5% bovine serum albumin (BSA) in TBS-T, respectively. The following antibodies were used: mouse monoclonal anti-pUL123 (IE1, 1:50 dilution), rabbit monoclonal anti-PERK (Cell Signaling; no. 3192, 1:600 dilution), monoclonal anti-ATF4 D4B8 (Cell Signaling; no. 11815, 1:600 dilution), rabbit polyclonal anti-ELOVL7 (Sigma-Aldrich; no. SAB3500390, 1:1,000 dilution), rabbit polyclonal anti-ELOVL5 (Sigma-Aldrich; no. SAB4502642, 1:500 dilution), rabbit polyclonal anti- β -actin (Proteintech; no. 20536-1-AP, 1:2,000 dilution), and mouse monoclonal anti- α -tubulin (Sigma-Aldrich; no. T6199, 1:2,000 dilution). Blots with mouse monoclonal anti-HCMV, anti-actin, and anti-tubulin antibodies were incubated for 1 h at room temperature. All others were incubated overnight at 4°C. Quantification of Western blots was performed using a LI-COR Odyssey CLx imaging system.

SUPPLEMENTAL MATERIAL

Supplemental material is available online only.

FIG S1, TIF file, 1 MB.

FIG S2, TIF file, 1.3 MB.

FIG S3, TIF file, 1.3 MB.

FIG S4, TIF file, 1.2 MB.

FIG S5, TIF file, 0.8 MB.

FIG S6, TIF file, 0.2 MB.

ACKNOWLEDGMENTS

We thank James Alwine for helpful feedback related to this project and critical reading of the paper. We thank Lisa Wise for valuable feedback pertaining to the lipidomic and knockout studies and Debbie Mustacich for assisting with CRISPR/Cas9 engineering.

This project was supported by startup funds from the University of Arizona Health Sciences, College of Medicine–Tucson, and the BIO5 Institute to J.G.P. Additional support for this work was provided by a New Investigator Award (ADHS18-198868) to J.G.P. from the Arizona Biomedical Research Commission, made available through the Arizona Department of Health Services.

REFERENCES

- Preiser JC, Ichai C, Orban JC, Groeneveld AB. 2014. Metabolic response to the stress of critical illness. *Br J Anaesth* 113:945–954. <https://doi.org/10.1093/bja/aeu187>.
- Rabasa C, Dickson SL. 2016. Impact of stress on metabolism and energy balance. *Curr Opin Behav Sci* 9:71–77. <https://doi.org/10.1016/j.cobeha.2016.01.011>.
- Han J, Kaufman RJ. 2016. The role of ER stress in lipid metabolism and lipotoxicity. *J Lipid Res* 57:1329–1338. <https://doi.org/10.1194/jlr.R067595>.
- Shenk T, Alwine JC. 2014. Human cytomegalovirus: coordinating cellular stress, signaling, and metabolic pathways. *Annu Rev Virol* 1:355–374. <https://doi.org/10.1146/annurev-virology-031413-085425>.
- Siddiquey MNA, Zhang H, Nguyen CC, Domma AJ, Kamil JP. 2018. The human cytomegalovirus endoplasmic reticulum-resident glycoprotein UL148 activates the unfolded protein response. *J Virol* 92:e00896-18. <https://doi.org/10.1128/JVI.00896-18>.
- Zhang H, Read C, Nguyen CC, Siddiquey MNA, Shang C, Hall CM, von Einem J, Kamil JP. 2019. The human cytomegalovirus nonstructural glycoprotein UL148 reorganizes the endoplasmic reticulum. *mBio* 10:e02110-19. <https://doi.org/10.1128/mBio.02110-19>.
- Yu Y, Pierciey FJ, Jr, Maguire TG, Alwine JC. 2013. PKR-like endoplasmic reticulum kinase is necessary for lipogenic activation during HCMV infection. *PLoS Pathog* 9:e1003266. <https://doi.org/10.1371/journal.ppat.1003266>.
- Xi Y, Harwood S, Wise L, Purdy JG. 2019. Human cytomegalovirus pUL37x1 is important to remodeling of host lipid metabolism. *J Virol* 93:e00843-19. <https://doi.org/10.1128/JVI.00843-19>.
- Bobrovnikova-Marjon E, Hatzivassiliou G, Grigoriadou C, Romero M, Cavener DR, Thompson CB, Diehl JA. 2008. PERK-dependent regulation of lipogenesis during mouse mammary gland development and adipocyte differentiation. *Proc Natl Acad Sci U S A* 105:16314–16319. <https://doi.org/10.1073/pnas.0808517105>.
- Yu Y, Maguire TG, Alwine JC. 2012. Human cytomegalovirus infection induces adipocyte-like lipogenesis through activation of sterol regulatory element binding protein 1. *J Virol* 86:2942–2949. <https://doi.org/10.1128/JVI.06467-11>.
- Spencer CM, Schafer XL, Moorman NJ, Munger J. 2011. Human cytomegalovirus induces the activity and expression of acetyl-coenzyme A carboxylase, a fatty acid biosynthetic enzyme whose inhibition attenuates viral replication. *J Virol* 85:5814–5824. <https://doi.org/10.1128/JVI.02630-10>.
- Munger J, Bennett BD, Parikh A, Feng XJ, McArdle J, Rabinowitz HA, Shenk T, Rabinowitz JD. 2008. Systems-level metabolic flux profiling identifies fatty acid synthesis as a target for antiviral therapy. *Nat Biotechnol* 26:1179–1186. <https://doi.org/10.1038/nbt.1500>.
- Purdy JG, Shenk T, Rabinowitz JD. 2015. Fatty acid elongase 7 catalyzes lipidome remodeling essential for human cytomegalovirus replication. *Cell Rep* 10:1375–1385. <https://doi.org/10.1016/j.celrep.2015.02.003>.
- Koyuncu E, Purdy JG, Rabinowitz JD, Shenk T. 2013. Saturated very long chain fatty acids are required for the production of infectious human cytomegalovirus progeny. *PLoS Pathog* 9:e1003333. <https://doi.org/10.1371/journal.ppat.1003333>.
- Ohno Y, Suto S, Yamanaka M, Mizutani Y, Mitsutake S, Igarashi Y, Sassa T, Kihara A. 2010. ELOVL1 production of C24 acyl-CoAs is linked to C24 sphingolipid synthesis. *Proc Natl Acad Sci U S A* 107:18439–18444. <https://doi.org/10.1073/pnas.1005572107>.
- Tamura K, Makino A, Hüllin-Matsuda F, Kobayashi T, Furihata M, Chung S, Ashida S, Miki T, Fujioka T, Shuin T, Nakamura Y, Nakagawa H. 2009. Novel lipogenic enzyme ELOVL7 is involved in prostate cancer growth through saturated long-chain fatty acid metabolism. *Cancer Res* 69:8133–8140. <https://doi.org/10.1158/0008-5472.CAN-09-0775>.
- Kitazawa H, Miyamoto Y, Shimamura K, Nagumo A, Tokita S. 2009. Development of a high-density assay for long-chain fatty acyl-CoA elongases. *Lipids* 44:765–773. <https://doi.org/10.1007/s11745-009-3320-8>.
- Ofman R, Dijkstra IM, van Roermund CW, Burger N, Turkenburg M, van Cruchten A, van Engen CE, Wanders RJ, Kemp S. 2010. The role of ELOVL1 in very long-chain fatty acid homeostasis and X-linked adrenoleukodystrophy. *EMBO Mol Med* 2:90–97. <https://doi.org/10.1002/emmm.201000061>.
- Leonard AE, Kelder B, Bobik EG, Chuang LT, Lewis CJ, Kopchick JJ, Mukerji P, Huang YS. 2002. Identification and expression of mammalian long-chain PUFA elongation enzymes. *Lipids* 37:733–740. <https://doi.org/10.1007/s11745-002-0955-6>.
- Jakobsson A, Westerberg R, Jacobsson A. 2006. Fatty acid elongases in mammals: their regulation and roles in metabolism. *Prog Lipid Res* 45:237–249. <https://doi.org/10.1016/j.plipres.2006.01.004>.
- Isler JA, Skalet AH, Alwine JC. 2005. Human cytomegalovirus infection activates and regulates the unfolded protein response. *J Virol* 79:6890–6899. <https://doi.org/10.1128/JVI.79.11.6890-6899.2005>.
- Xuan B, Qian Z, Torigoi E, Yu D. 2009. Human cytomegalovirus protein pUL38 induces ATF4 expression, inhibits persistent JNK phosphorylation, and suppresses endoplasmic reticulum stress-induced cell death. *J Virol* 83:3463–3474. <https://doi.org/10.1128/JVI.02307-08>.
- Bobrovnikova-Marjon E, Pytel D, Riese MJ, Vaites LP, Singh N, Koretzky GA, Witze ES, Diehl JA. 2012. PERK utilizes intrinsic lipid kinase activity to generate phosphatidic acid, mediate Akt activation, and promote adipocyte differentiation. *Mol Cell Biol* 32:2268–2278. <https://doi.org/10.1128/MCB.00063-12>.
- Lee AH, Glimcher LH. 2009. Intersection of the unfolded protein response and hepatic lipid metabolism. *Cell Mol Life Sci* 66:2835–2850. <https://doi.org/10.1007/s00018-009-0049-8>.
- Sanchez V, Dong JJ. 2010. Alteration of lipid metabolism in cells infected with human cytomegalovirus. *Virology* 404:71–77. <https://doi.org/10.1016/j.virol.2010.04.026>.
- Vysochan A, Sengupta A, Weljie AM, Alwine JC, Yu Y. 2017. ACS2-mediated acetyl-CoA synthesis from acetate is necessary for human cytomegalovirus infection. *Proc Natl Acad Sci U S A* 114:E1528–E1535. <https://doi.org/10.1073/pnas.1614268114>.
- Naganuma T, Sato Y, Sassa T, Ohno Y, Kihara A. 2011. Biochemical characterization of the very long-chain fatty acid elongase ELOVL7. *FEBS Lett* 585:3337–3341. <https://doi.org/10.1016/j.febslet.2011.09.024>.

28. Rodriguez-Sanchez I, Munger J. 2019. Meal for two: human cytomegalovirus-induced activation of cellular metabolism. *Viruses* 11:273. <https://doi.org/10.3390/v11030273>.
29. Lange PT, Lagunoff M, Tarakanova VL. 2019. Chewing the fat: the conserved ability of DNA viruses to hijack cellular lipid metabolism. *Viruses* 11:119. <https://doi.org/10.3390/v11020119>.
30. Sanchez EL, Lagunoff M. 2015. Viral activation of cellular metabolism. *Virology* 479–480:609–618. <https://doi.org/10.1016/j.virol.2015.02.038>.
31. Purdy JG, Luftig MA. 2019. Reprogramming of cellular metabolic pathways by human oncogenic viruses. *Curr Opin Virol* 39:60–69. <https://doi.org/10.1016/j.coviro.2019.11.002>.
32. Basseri S, Austin RC. 2012. Endoplasmic reticulum stress and lipid metabolism: mechanisms and therapeutic potential. *Biochem Res Int* 2012:841362. <https://doi.org/10.1155/2012/841362>.
33. Fu S, Watkins SM, Hotamisligil GS. 2012. The role of endoplasmic reticulum in hepatic lipid homeostasis and stress signaling. *Cell Metab* 15:623–634. <https://doi.org/10.1016/j.cmet.2012.03.007>.
34. Sharon-Friling R, Goodhouse J, Colberg-Poley AM, Shenk T. 2006. Human cytomegalovirus pUL37x1 induces the release of endoplasmic reticulum calcium stores. *Proc Natl Acad Sci U S A* 103:19117–19122. <https://doi.org/10.1073/pnas.0609353103>.
35. Dejeans N, Tajeddine N, Beck R, Verrax J, Taper H, Gailly P, Calderon PB. 2010. Endoplasmic reticulum calcium release potentiates the ER stress and cell death caused by an oxidative stress in MCF-7 cells. *Biochem Pharmacol* 79:1221–1230. <https://doi.org/10.1016/j.bcp.2009.12.009>.
36. Liu ST, Sharon-Friling R, Ivanova P, Milne SB, Myers DS, Rabinowitz JD, Brown HA, Shenk T. 2011. Synaptic vesicle-like lipidome of human cytomegalovirus virions reveals a role for SNARE machinery in virion egress. *Proc Natl Acad Sci U S A* 108:12869–12874. <https://doi.org/10.1073/pnas.1109796108>.
37. Parisi LR, Sowlati-Hashjin S, Berhane IA, Galster SL, Carter KA, Lovell JF, Chemler SR, Karttunen M, Atilla-Gokcumen GE. 2019. Membrane disruption by very long chain fatty acids during necroptosis. *ACS Chem Biol* 14:2286–2294. <https://doi.org/10.1021/acscchembio.9b00616>.
38. Parisi LR, Li N, Atilla-Gokcumen GE. 2017. Very long chain fatty acids are functionally involved in necroptosis. *Cell Chem Biol* 24:1445–1454.e8. <https://doi.org/10.1016/j.chembiol.2017.08.026>.
39. Brune W, Andoniou CE. 2017. Die another day: inhibition of cell death pathways by cytomegalovirus. *Viruses* 9:249. <https://doi.org/10.3390/v9090249>.
40. Guo H, Kaiser WJ, Mocarski ES. 2015. Manipulation of apoptosis and necroptosis signaling by herpesviruses. *Med Microbiol Immunol* 204:439–448. <https://doi.org/10.1007/s00430-015-0410-5>.
41. Green CD, Olson LK. 2011. Modulation of palmitate-induced endoplasmic reticulum stress and apoptosis in pancreatic beta-cells by stearoyl-CoA desaturase and Elovl6. *Am J Physiol Endocrinol Metab* 300:E640–E649. <https://doi.org/10.1152/ajpendo.00544.2010>.
42. Micoogullari Y, Basu SS, Ang J, Weisshaar N, Schmitt ND, Abdelmoula WM, Lopez B, Agar JN, Agar N, Hanna J. 2020. Dysregulation of very-long-chain fatty acid metabolism causes membrane saturation and induction of the unfolded protein response. *Mol Biol Cell* 31:7–17. <https://doi.org/10.1091/mbc.E19-07-0392>.
43. Pineau L, Ferreira T. 2010. Lipid-induced ER stress in yeast and beta cells: parallel trails to a common fate. *FEMS Yeast Res* 10:1035–1045. <https://doi.org/10.1111/j.1567-1364.2010.00674.x>.
44. Deguil J, Pineau L, Rowland Snyder EC, Dupont S, Beney L, Gil A, Frapper G, Ferreira T. 2011. Modulation of lipid-induced ER stress by fatty acid shape. *Traffic* 12:349–362. <https://doi.org/10.1111/j.1600-0854.2010.01150.x>.
45. Kilberg MS, Shan J, Su N. 2009. ATF4-dependent transcription mediates signaling of amino acid limitation. *Trends Endocrinol Metab* 20:436–443. <https://doi.org/10.1016/j.tem.2009.05.008>.
46. Harding HP, Zhang Y, Zeng H, Novoa I, Lu PD, Calfon M, Sadri N, Yun C, Popko B, Paules R, Stojdl DF, Bell JC, Hettmann T, Leiden JM, Ron D. 2003. An integrated stress response regulates amino acid metabolism and resistance to oxidative stress. *Mol Cell* 11:619–633. [https://doi.org/10.1016/s1097-2765\(03\)00105-9](https://doi.org/10.1016/s1097-2765(03)00105-9).
47. Fusakio ME, Willy JA, Wang Y, Mirek ET, Al Baghdadi RJ, Adams CM, Anthony TG, Wek RC. 2016. Transcription factor ATF4 directs basal and stress-induced gene expression in the unfolded protein response and cholesterol metabolism in the liver. *Mol Biol Cell* 27:1536–1551. <https://doi.org/10.1091/mbc.E16-01-0039>.
48. Wang C, Huang Z, Du Y, Cheng Y, Chen S, Guo F. 2010. ATF4 regulates lipid metabolism and thermogenesis. *Cell Res* 20:174–184. <https://doi.org/10.1038/cr.2010.4>.
49. Ren LP, Yu X, Song GY, Zhang P, Sun LN, Chen SC, Hu ZJ, Zhang XM. 2016. Impact of activating transcription factor 4 signaling on lipogenesis in HepG2 cells. *Mol Med Rep* 14:1649–1658. <https://doi.org/10.3892/mmr.2016.5453>.
50. Chen H, Yuan R, Zhang Y, Zhang X, Chen L, Zhou X, Yuan Z, Nie Y, Li M, Mo D, Chen Y. 2016. ATF4 regulates SREBP1c expression to control fatty acids synthesis in 3T3-L1 adipocytes differentiation. *Biochim Biophys Acta* 1859:1459–1469. <https://doi.org/10.1016/j.bbagr.2016.07.010>.
51. Keo A, Mahfouz A, Ingrassia AMT, Meneboo JP, Villenet C, Mutez E, Comptdaer T, Lelieveldt BPF, Figeac M, Chartier-Harlin MC, van de Berg WDJ, van Hilten JJ, Reinders MJT. 2020. Transcriptomic signatures of brain regional vulnerability to Parkinson's disease. *Commun Biol* 3:101. <https://doi.org/10.1038/s42003-020-0804-9>.
52. Sinzger C, Hahn G, Digel M, Katona R, Sampaio KL, Messerle M, Hengel H, Koszinowski U, Brune W, Adler B. 2008. Cloning and sequencing of a highly productive, endotheliotropic virus strain derived from human cytomegalovirus TB40/E. *J Gen Virol* 89:359–368. <https://doi.org/10.1099/vir.0.83286-0>.
53. Umashankar M, Petrucelli A, Cicchini L, Caposio P, Kreklywich CN, Rak M, Bughio F, Goldman DC, Hamlin KL, Nelson JA, Fleming WH, Streblov DN, Goodrum F. 2011. A novel human cytomegalovirus locus modulates cell type-specific outcomes of infection. *PLoS Pathog* 7:e1002444. <https://doi.org/10.1371/journal.ppat.1002444>.
54. Yu D, Smith GA, Enquist LW, Shenk T. 2002. Construction of a self-excisable bacterial artificial chromosome containing the human cytomegalovirus genome and mutagenesis of the diploid TRL/IRL13 gene. *J Virol* 76:2316–2328. <https://doi.org/10.1128/jvi.76.5.2316-2328.2002>.
55. Read C, Schauflinger M, Nikolaenko D, Walther P, von Einem J. 2019. Regulation of human cytomegalovirus secondary envelopment by a C-terminal tetralysine motif in pUL71. *J Virol* 93:e02244-18. <https://doi.org/10.1128/JVI.02244-18>.
56. Konig P, Svrlanska A, Read C, Feichtinger S, Stamminger T. 2020. The autophagy-initiating protein kinase ULK1 phosphorylates human cytomegalovirus tegument protein pp28 and regulates efficient virus release. *J Virol* 95:e02346-20. <https://doi.org/10.1128/JVI.02346-20>.
57. Sanjana NE, Shalem O, Zhang F. 2014. Improved vectors and genome-wide libraries for CRISPR screening. *Nat Methods* 11:783–784. <https://doi.org/10.1038/nmeth.3047>.
58. Shalem O, Sanjana NE, Hartenian E, Shi X, Scott DA, Mikkelsen T, Heckl D, Ebert BL, Root DE, Doench JG, Zhang F. 2014. Genome-scale CRISPR-Cas9 knockout screening in human cells. *Science* 343:84–87. <https://doi.org/10.1126/science.1247005>.
59. Cappadona I, Villinger C, Schutzius G, Mertens T, von Einem J. 2015. Human cytomegalovirus pUL47 modulates tegumentation and capsid accumulation at the viral assembly complex. *J Virol* 89:7314–7328. <https://doi.org/10.1128/JVI.00603-15>.
60. Dietz AN, Villinger C, Becker S, Frick M, von Einem J. 2017. A tyrosine-based trafficking motif of the tegument protein pUL71 is crucial for human cytomegalovirus secondary envelopment. *J Virol* 92:e00907-17. <https://doi.org/10.1128/JVI.00907-17>.
61. Melamed E, Vastag L, Rabinowitz JD. 2010. Metabolomic analysis and visualization engine for LC-MS data. *Anal Chem* 82:9818–9826. <https://doi.org/10.1021/ac1021166>.